Application of the Period Dependence of Stability Coefficient in Enhancement of Seismic Design and Evaluation of Seismic Response under Biaxial Excitation

Seyed Mohammad Fard Mousavi

Submitted to the
Institute of Graduate Studies and Research
in Partial fulfillment of the requirement for the degree of

Doctor of Philosophy
in
Civil Engineering

Eastern Mediterranean University
July 2019,
Gazimağusa, North Cyprus

Approval of the Institute of Graduate Studies and Research

Prof. Dr. Ali Hakan Ulusoy
Acting Director

I certify that this thesis satisfies the requirements as a thesis for the degree of Doctor of Philosophy in Civil Engineering.

Assoc. Prof. Dr. Serhan Şensoy
Chair, Department of Civil Engineering

We certify that we have read this thesis and that in our opinion it is fully adequate in scope and quality as a thesis for the degree of Doctor of Philosophy in Civil Engineering.

Assoc. Prof. Dr. Serhan Şensoy
Supervisor

Examining Committee

1. Prof. Dr. Cenk Alhan _____
2. Prof. Dr. Özgür Eren _____
3. Prof. Dr. Haluk Sucuoğlu _____
4. Assoc. Prof. Dr. Giray Özay _____
5. Assoc. Prof. Dr. Serhan Şensoy _____

ABSTRACT

Present study tries to simplify seismic resistance design process based on the stability coefficient (SC) and /or displacement (rotation) limits defined by practicing codes. To this end, a constant ductility response spectrum, derived for the first story with total mass acting on it, and known height, in which the P-delta effect and period-dependent feature of the SC is exclusively inherent, is used. The mentioned spectrum plots spectral acceleration, or yield displacement (rotation), versus SC, and hence, is referred to as the "stability-coefficient-response-spectra". The notion of the "first-storey-single-degree-of-freedom" (FSSDOF) system is presented next. The FSSDOF is intended to set the minimum necessary lateral stiffness complying with a pre-specified ductility level at early stages of design. Moreover, the pendulum model is used to evaluate effects of the geometric-nonlinearity and vertical-component-of-ground-motion (VCGM) on the global-inelastic-response of non-deteriorating bilinear single-degree-of-freedom (SDOF) systems. Results indicate that both VCGM and geometric nonlinearity affect the inelastic response, which are significant for certain combinations of the initial period of vibration, strength reduction factor and ductility demand. In addition, effect of the VCGM is not limited to near fault regions. Furthermore, it is shown that the VCGM could cause dynamic instability of SDOF systems; hence, given the importance of SDOF systems in evaluation of existing structures, considering the VCGM for collapse assessment is suggested.

Keywords: P-delta effect, stability-coefficient-response-spectra, first-storey-single-degree-of-freedom system, vertical-component-of-ground-motion, geometric nonlinearity, response/design spectrum.

ÖZ

Bu çalışmada depreme dayanıklı yapı tasarımında mevcut depreme dayanıklı yapı tasarımı yönetmeliklerinde belirtilen ikinci mertebe gösterge değeri (İMGD) ve yer değiştirme sınırlarını dikkate alarak basit bir yöntemin ortaya konulmasına çalışılmıştır. Bu doğrultuda belli bir süneklilik değerine bağlı spektrumlar, birinci kata gelen toplam kütle ve belli bir yükseklik için ikinci mertebe gösterge değerinin periyoda bağlı özelliği de göz önüne alınarak oluşturulmuş ve kullanılmıştır. Yukarıda belirtilen spektrum her İMGD değerine karşı gelen spektral ivme veya akma deplasmanı (şekil değiştirme) çizelgesi olarak sunulmuş ve bu nedenle "İkinci Mertebe gösterge değeri-etki spektrumu" olarak belirtilmiştir. Bu çalışma kapsamında "Birinci kat tek serbestlik dereceli" (BKTSD) sistemler ele alınmıştır. BKTSD sistem önceden belirlenen süneklik oranının korunması için gerekli en düşük yatay rijitliğin belirlenmesine olanak sağlayarak tasarımın erken evrelerinde kullanılabilmektedir. Buna ilaveten bozulmayan bilinear elastik olmayan tek serbestlik dereceli ters sarkaç modelleri geometrik nonlineerlik etkisinin ve deprem düşey bileşeni (DDB) etkisinin belirlenmesine olanak sağlamaktadır. Sonuçlar DDB ve geometrik nonlineerlik etkilerinin özellikle bazı başlangıç doğal titreşim periyoduna, süneklik düzeyine ve davranış katsayısının bileşenlerinde önemli etkiye sahip olduğu belirlenmiştir. Ayrıca DDB etkisinin sadece yakın faylar tarfından üretilen depremlerde etkili olmadığı gözlemlenmiştir. Tüm bunlara ilaveten DDB etkisinin dinamik kararsızlığa neden olabileceği ve bu nedenle tek serbestlik dereceli olarak modellenen sistemlerin göçme durumlarının belirlenmesinde dikkate alınması gerektiği önerilmektedir.

Anahtar Kelimeler: ikinci mertebe etki, ikinci mertebe gösterge değeri-etki spektrumu, birinci kat tek serbestlik dereceli sistem, deprem düşey bileşeni, geometrik nonlineerite, etki/tasarım spektrumu.

To My Love…

ACKNOWLEDGMENT

There are several people who deserve to be publicly thanked and acknowledged for their help and inspiration during my PhD studies. First, I would like to express my deep gratitude to Associate Professor Serhan Şensoy, my supervisor, for his enthusiastic encouragement and wholehearted support. I would also like to extend my appreciation to Professor Özgür Eren for his unconditional care towards my improvements. In addition, my sincere gratitude goes to all my thesis committee members for their insightful comments and valuable recommendations.

I am also thankful to the entire civil engineering academic and administrative staff. I would like to heart-fully acknowledge Dr. Amir Bahador Nataj, for fruitful discussions and encouragement during my PhD studies.

I would also like to thank my beloved parents and parents-in-law for their support throughout my studies. My special appreciation goes to Professor Mehdi Baradarani who had an unshakeable belief in my abilities.

Nobody has been more important to me in the pursuit of this research than my wife, Sarvnaz Baradarani. Understanding me best as a PhD herself, she has been my best friend and great companion, loved, supported, encouraged and helped me get through this period in the most positive way.

TABLE OF CONTENTS

LIST OF TABLES

LIST OF FIGURES

LIST OF SYMBOLS

m	Mass
h	Height
$M(\emptyset)$	Rotational Resistance of the Spring
P	Vertical Load
$\emptyset$	Generalized Coordinate; Deviation of the Pendulum from Vertical Axis
$\ddot{x}_h$	Horizontal Ground Acceleration
$\ddot{x}_v$	Vertical Ground Acceleration
$c_\emptyset$	Damping Parameter
Δ	Lateral Displacement
V	Lateral Load
θ	Stability Coefficient
$K_{\emptyset 0}$	Initial Rotational Stiffness of the Spring (without P-delta)
$K_\emptyset$	Apparent Rotational Stiffness of the Spring (with P-delta)
$K_{\Delta 0}$	Initial Lateral Stiffness of the Spring (without P-delta)
K_Δ	Apparent Lateral Stiffness of the Spring (with P-delta)
g	Acceleration of Gravity
ω_0	Initial Circular Frequency (without P-delta)
ω	Apparent Circular Frequency (with P-delta)
T_0	Initial Period of Vibration (without P-delta)
ω_G^2	Geometric Frequency
a	The spring's Hardening
z	New State Variable for Modeling the Hysteric Behavior
$\emptyset_y$	Yield Rotation

n	Parameter Controlling the Hysteric Curve
β_1	Parameter Controlling the Hysteric Curve
β_2	Parameter Controlling the Hysteric Curve
$M(s)$	Apparent Stiffness of the System
ν	Amplitude of the Harmonic Excitation
Ω	Frequency of the Harmonic Excitation
R	Strength Reduction Factor
μ	Ductility
M_i	Accumulated Seismic Mass Above the i^{th} Level
A	Spectral Acceleration
D	Spectral Displacement
θ_V	Stability Coefficient in Presence of the Vertical Ground Acceleration
ω_{GV}^2	Geometric Frequency in Presence of the Vertical Ground Acceleration

LIST OF ABBREVIATIONS

DBD	Displacement Based Design
DDBD	Direct Displacement Based Design
ESDOF	Equivalent Single-Degree-of-Freedom
FSSDOF	First-Storey-Single-Degree-of-Freedom
MDOF	Multi-Degree-of-Freedom
MSD	Mass-Spring-Damper
NPYS	Negative-Post-Yield-Stiffness
PPYS	Positive-Post-Yield-Stiffness
SC	Stability Coefficient
SCB	Strength Based Design
SCRS	Stability Coefficient Response Spectra
SDOF	Single-Degree-of-Freedom
UPEM	Unified Piece-Wise Exact Method
VCGM	Vertical-Component-of-Ground-Motion

Chapter 1

INTRODUCTION

1.1 Preface

With increasing knowledge on behavior of structures, and nature of earthquakes, seismic design of structures has gone through a number of fundamental improvements during the last century. Starting from simple mass proportional lateral forces, it continued to recognize influence of period in modifying inertia forces, ductility, in resisting more intense disturbances, and drifts, in controlling potential damages (Priestley, Calvi, & Kowalsky, 2007). In light of various pioneering studies, two major design methodologies have gained global acceptance, namely: strength/force-based-design (SBD) and displacement-based-design (DBD) methods. While in a strength/force-based approach emphasize is on the necessary strength conforming to a given ductility level, displacement-based design methods debate that to limit potential damages, controlling structural deformations is a better approach (Priestley, 2000). Nevertheless, both abovementioned methods have a common problem to solve; that is, how second-order-effects resulting from action of gravity loads going through lateral displacements, the so-called P-delta effect (Christoph Adam, Ibarra, & Krawinkler, 2004; Rahimi & Estekanchi, 2015), should be counterbalanced.

On the other hand, previous literature indicates that effect of Vertical-Component-of-Ground-Motion (VCGM) on seismic response of structures might be very

significant, with devastating results in certain cases (Elnashai & Papazoglou, 1997). In response to such effects, some of the modern seismic design practicing codes have started to recognize effect of VCGM (CEN, 2005; FEMA, 2009; TEC, 2018). This is done by providing guidelines for construction of a new response spectrum in vertical direction. The mentioned spectrum, however, is based on a mass-spring-damper (MSD) vibrator in vertical direction. Obviously, uncoupling earthquake components may not perfectly resemble state of a structure during a strong ground motion. Therefore, examining behavior of structures under coupled action of earthquake components is important.

Studying the effect of the VCGM is inter-related with P-delta effect, since variations of the gravitational acceleration may alter response of a system vulnerable to destabilizing secondary effects. Henceforth, present study follows a twofold aim. Its first goal is to enhance inclusion of the P-delta effect in the design procedure. This is done by means of combining several previously proposed notions. Specifically, it tries to give a realistic estimation on the minimum necessary lateral stiffness, complying with a given level of ductility, in which P-delta effect is exclusively considered. To this end, two new concepts are introduced, namely: the *"stability coefficient response spectra"* (SCRS), and, the *"first-storey-single-degree-of-freedom"* (FSSDOF) system.

The SCRS is a constant ductility response spectrum in terms of the stability-coefficient (SC) versus spectral acceleration. Alternatively, it can be plotted in terms of any other desired spectral information; for instance, spectral displacement. FSSDOF system is basically an especial single-degree-of-freedom (SDOF) system, utilized to the first-storey of a given Multi-Degree-of-Freedom (MDOF) system,

with known height. Therefore, “an alternative response/design spectrum”, with further practical advantages, will result (see Chapter 5).

Both aforementioned notions are developed based on the governing equation of motion of an inverted-pendulum model. This is done since shortcomings of the MSD models, as “the SDOF” system, in simulating state of a structure in deformed configuration have long been recognized. By use of an inverted-pendulum model, explicit consideration of the P-delta effect is facilitated; while all the necessary requirements of a SDOF system are satisfied.

Such a treatment also permits inclusion of the VCGM in derivation of the response/design spectrum, as well as, consideration of the “geometric nonlinearity” at global level. Specifically speaking, upon consideration of geometric nonlinearity, it can be seen that effects of the P-delta and VCGM on a system’s response are similar (see chapter 2). Therefore, and as secondary objectives, present study systematically evaluates effect of geometric nonlinearity and VCGM on the global response of SDOF systems.

To achieve above-mentioned goals, however, a broad understanding of the effects of P-delta and VCGM on global response is necessary. Hence, a relatively comprehensive discussion on the previous literature regarding P-delta effect and VCGM is presented next.

1.2 P-delta Effect

One important mode of failure of structures is associated with gravity loads undergoing lateral displacements upon action of ground motion (the so-called global P-delta effect) (Rahimi & Estekanchi, 2015). Although inclusion of the P-delta effect

into the both above mentioned design procedures has been the focus of many studies (Bernal, 1998; MacRae, 1994; Tjondro, Moss, & Carr, 1992), developing robust methods to achieve reliable results is still attractive. For example, one can name (Belleri, Torquati, Marini, & Riva, 2017; López, Ayala, & Adam, 2015), as recent proposals for treating P-delta effect in a displacement-based context, and (Amara, Bosco, Marino, & Rossi, 2014), as a recent effort in a strength-based context.

P-delta effect, has usually been quantified through SC (sometimes referred to as "stability index" or "inter-storey drift sensitivity index"). It reduces lateral resistance of a system, which under strong excitation may cause loss of load carrying capacity (Gupta & Krawinkler, 2000). For elastic systems under static loading, P-delta effect causes elongation of period (reduction of stiffness). However, for inelastic response, and under dynamic excitation, its effect becomes complicated.

Several pioneering studies focused on proposing strategies to ensure safety against P-delta effect (Jennings & Husid, 1968; Miranda & Akkar, 2003; Sun, Berg, & Hanson, 1973; Williamson, 2003).

Some scholars have suggested that, if SC is kept sufficiently small (i.e. stiffness is adequately increased), P-delta effect can safely be ignored (Andrews, 1977; MacRae, 1994). However, such a strategy demands for several trials that is: after increasing lateral stiffness, fundamental period of vibration will change and hence a new set of lateral forces should be calculated. Moreover, since the restriction on SC is not directly imposed on the fundamental period of vibration, after calculating a preliminary base-shear the procedure should be repeated without knowing how much increase in lateral stiffness is actually required. In some of the previously conducted

studies, it had been noted that the mentioned strategy potentially forces towards constant region of a design spectrum, with maximum response (MacRae, 1994). Thus, it had been argued that increasing strength, instead of stiffness, may solve the problem (Paulay, 1978). Nevertheless, later studies showed that there is a relation between strength and stiffness (Priestley, 2000); i.e., changes in one property induces changes in the other one.

Great efforts have been exercised to include P-delta effect into the design procedure in a more direct manner. Some studies have argued that P-delta effect can be satisfactorily compensated by incorporating strength/displacement amplification factors (Wei, Xu, & Li, 2011). Amplification factors are used to ensure that ductility demand in presence and absence of P-delta effect remain same. Bernal (1987), suggested that ratio of inelastic constant ductility response spectrum constructed for the cases with and without P-delta effect can be used to amplify stiffness. For a system with known ductility and SC, a general formula was regressed for direct derivation of amplification factors (Bernal, 1987).

Although there are various different suggestions for derivation of amplification factors (MacRae, 1994; Rosenblueth, 1965), generalization of such an approach is very complicated. This is mainly because of variety of influential parameters, (Amara et al., 2014), and nonlinear relation between strength reduction factor and ductility demand (Aschheim & Montes, 2003). Hence, it is not surprising that every often code specified amplification factors are subjected to criticism. For instance, Amara et al. (2014) have shown that (ASCE/SEI, 2010) provisions tend to underestimate strength amplification factors, while those of Euro Code 8 (CEN, 2005) are conservative.

On the other hand, inclusion of P-delta effect in direct-displacement-based-design (DDBD) context has also been the focus of several studies. In DDBD method the original MDOF system is represented by an Equivalent-Single-Degree-of-Freedom (ESDOF) system (Priestley et al., 2007). Hence, one needs a unique SC for the whole MDOF system while it is usually defined at each storey (Asimakopoulos, Karabalis, & Beskos, 2007). To overcome this problem, in some studies pushover analysis is used for derivation of a global inelastic SC (e.g. (L. F. Ibarra & Krawinkler, 2004; L. F. Ibarra, Medina, & Krawinkler, 2005; Miranda & Akkar, 2003)). Black (2011), proposed the concept of "Modal Inelastic Stability Coefficient" by recognizing effect of height in representing the ESDOF system. Asimakopoulos et al. (2007), proposed that the maximum value of SC over the total height of a MDOF system under dynamic loading – the so-called dynamic SC – can be considered as a good estimator for the SC of the ESDOF system. Based on results of several time history analyses, they derived a general formula for SC of moment resisting steel frames. They concluded that, EuroCode 8 amplification factors underestimate P-delta effect (a result in contrast with (Amara et al., 2014)).

Reflection of previous studies on seismic resistance codes is a combination of previously proposed strategies. For example, according to EuroCode 8 , ASCE7-10, and Turkish Standards (ASCE/SEI, 2010; CEN, 2005; TEC, 2018), P-delta effect can be neglected if SC is sufficiently small. To neglecting P-delta effect, EC8 and ASCE7-10 demand for the SC to be less than 0.1, while Turkish Standards limit is 0.12. The first two specifications allow counterbalancing P-delta effect by amplifying lateral forces/displacements if SC is larger than 0.1, but less than 0.25, and 0.3, in ASCE7-10, and EC8, respectively. If the SC is larger than the above-

mentioned limits, lateral stiffness of the structure should be adjusted to bring it to one of the previous conditions.

Having said this, P-delta effect (sometimes referred to as geometric nonlinearity) has usually been taken as a linear reduction in rotational stiffness (L. Ibarra & Krawinkler, 2011). The mentioned representation arises from an assumption which is: linearization of equation of motion introduces negligible errors in calculating the response (Bernal, 1987). Upon linearization, material behavior and P-delta effect are collectively embodied into the equation of motion of an equivalent single-degree-of-freedom system, which is considered to be representative of dynamic characteristics of a multi-degree-of-freedom system (Papadrakakis, Fragiadakis, Lagaros, & Plevris, 2011). Depending on relative values of stability coefficient and material hardening, P-delta effect may result in positive, zero, or negative-post-yield-stiffness (NPYS).

Previous studies, however, were mostly focused on systems experiencing NPYS. For example, it has been argued that P-delta effect is associated with development of NPYS and is especially important for flexible structures which are expected to experience large displacements under sever ground shaking (Gupta & Krawinkler, 2000). Effect of period of oscillation and post-yield stiffness on the necessary lateral strength to evade instability of SDOF systems by using relatively large values of SC has been conducted by Miranda and Akkar (2003). In that study, it was debated that NPYS might also arise due to degradation of material or a combination of P-delta and material degradation; hence, SC does not necessarily remain small. As it is clear from above discussion, systems which do not experience NPYS have received lesser attention. This is mainly because they are not expected to experience dynamic instability (Miranda & Akkar, 2003). Moreover, response of such systems is

considered to change insignificantly by presence of the P-delta effect. For instance, FEMA specification assigns a value of "one" to the P-delta related coefficient in displacement coefficient method (FEMA, 2009).

Obviously when calculating maximum inelastic displacement (rotation) is aimed, underlying assumption which permits linearization is violated. This is because maximum displacement does not need to actually happen; instead it gives a measure of the demand being imposed on the system.

1.3 Vertical Component of Ground Motion

With increasing evidence on ruinous effects of the VCGM, many studies focused on revealing its engineering characteristics (Elgamal & He, 2004), presenting analytical support for destructive field observations (Papazoglou & Elnashai, 1996), as well as proposing simplified peak ground acceleration, peak ground velocity and response spectra models to be implemented in seismic codes (Bozorgnia & Campbell, 2016; Çağnan, Akkar, Kale, & Sandıkkaya, 2017; Campbell, 2003; Campbell & Bozorgnia, 2003; Elnashai & Papazoglou, 1997).

Traditionally, VCGM has been described based on ratio of peak vertical ground acceleration to the peak horizontal one (V/H). Newmark, Blume, and Kapur (1973), suggested that a scaled version of horizontal design spectrum can be used in vertical direction by setting V/H to 2/3. In later studies, deficiencies of the 2/3 rule were indicated mainly because of two reasons. First, assuming same spectral shape is not consistent with dissimilarities in frequency content of the vertical and horizontal components of ground motion. Second, V/H ratio strongly depends on distance from fault and above rule underestimates at near-fault regions (Bozorgnia & Campbell,

2004; Collier & Elnashai, 2001). In addition to distance from source, V/H was found to be related to natural period and soil condition, while faulting mechanism and magnitude were found to have weak relation with V/H (Bozorgnia & Campbell, 2004; Campbell, 2003; Campbell & Bozorgnia, 2003).

While many of previous studies were focused on uncoupled action of vertical and horizontal components of ground motion, combined action of earthquake components has been the focus of a few studies (Rabiei & Khoshnoudian, 2011). For instance, Hjelmstad and Williamson (1998), used an inverted-pendulum to study dynamic instability of SDOF systems under bi-axial (horizontal and vertical) base excitation. By using the well-known "Mathew" equation, they showed that inclusion of near periodic vertical excitation may cause parametric resonance (also see (Williamson & Hjelmstad, 2001)). In their study,Graizer and Kalkan (2008), formulated the governing equation of motion of an inverted pendulum under complex inputs. By comparing responses of inverted pendulum model with its corresponding mass-spring model they found that the VCGM causes elongation of the period of vibration. Their findings are in agreement with results of (Kim, Holub, & Elnashai, 2010), who reported substantial variations in horizontal and vertical periods of vibration upon action of the VCGM. Graizer and Kalkan (2008), used an inverted pendulum to address coupled action of P-delta effect and VCGM. They asserted that P-delta effect might be magnified, reduced, or remain same upon action of VCGM (also see (Kalkan & Graizer, 2007)). This phenomenon was attributed to variations of the gravitational acceleration upon action of the VCGM. Ghaffarzadeh and Nazeri (2015) showed that combined action of the P-delta effect and VCGM could cause variations in the inelastic-horizontal-response, which is significant for certain initial periods. They used a two-degree-of-freedom system by appropriately

modifying the stiffness part of the equation of motion in the lateral direction to resemble the effects of the VCGM. Their model uses elastic behavior in vertical direction.

1.4 Aims and Objectives

Based on preceding discussions some important questions may arise:

- Presenting P-delta effect through a linearized equation of motion, although substantially simplifies derivation of the solution, may result in biased response. To the best of the author's knowledge, a systematic evaluation of potential effects of inclusion of the geometric nonlinearity at global level on the maximum-inelastic-response of SDOF systems is missing in current literature.
- On the other hand, effect of variation of the gravitational acceleration due to action of the VCGM and its influence on the P-delta effect, and in turn, on the maximum-inelastic-response has received lesser attention.
- Quantifying P-delta through SC brings up a problem that is; derivation of the base shear and lateral forces are based on fundamental period of vibration. However, story-wise SC checks impose an upper limit on individual story periods, not fundamental period. This fact makes accounting for the P-delta indirect and in a trial and error manner.

Based on above specified gaps, present study aims to:

- Evaluate effect of the geometric nonlinearity at global level on the inelastic response of SDOF systems,

- Evaluate effect of the VCGM on the maximum-inelastic-response, and specifically, its effect at far field distances and its capability to initiate dynamic instability,
- Present an alternative design/response spectrum based on the SCRS and FSSDOF to enhance the seismic design procedure.

1.5 Guide to the Thesis

After introduction, the second chapter presents the governing equation of motion and fundamental backgrounds for the study.

The third chapter is devoted to evaluation of effects of geometric nonlinearity on the global response. The discussion is categorized into two subsections based on whether SC is equal to, or greater than hardening. Effect of geometric nonlinearity for systems with the same hardening and SC is evaluated by comparing their corresponding estimates of the well-known ductility demand (Chopra, 2007). Comparisons are done for several harmonic excitations as well as the FEMA P-695 far field set of records (C. Haselton et al., 2012). When SC is greater than hardening, behaviors of systems are compared near to, and, at the collapse state. Again, both harmonic excitations and real recorded motions are used for analysis.

Forth chapter introduces the SCRS and the FSSDOF system. Based on presented notions, it is argued that an alternative response/design spectrum can be developed, which greatly enhances inclusion of P-delta effect into the both strength-based and displacement-based design methods. Several numerical examples are worked as part of presentation.

Fifth chapter discusses the effect of VCGM on global response of SDOF systems. It is worth noting that since SDOF systems are defined based on inverted-pendulum model, both VCGM and P-delta effect are present in analysis. However, their corresponding effects are distinguished by including P-delta effect into the analysis in presence and absence of the VCGM.

Finally, based on presented developments and discussions, the sixth chapter presents some concluding remarks.

Chapter 2

FRAME WORK AND FUNDAMENTALS

2.1 Equation of Motion

As stated earlier, MSD models cannot resemble the state of a structure in deformed position (i.e. cannot simulate P-delta effect). Having said this, some scholars have indicated that P-delta effect might be adequately simulated if the stiffness part of the governing equation of motion of a MSD model is appropriately adjusted (Bernal, 1987; MacRae, 1994). On the other hand, some studies suggested an inverted-pendulum model as an alternative for the MSD model (Graizer & Kalkan, 2008; Hjelmstad & Williamson, 1998). In this way, not only all the necessary requirements of SDOF systems are satisfied, but also P-delta effect is inherent in the governing equation of motion.

Referring to Figure (2.1), equation of motion of an inverted pendulum under biaxial excitation can be written as:

$$mh^2\ddot{\emptyset} - (P + m\ddot{x}_v)h\sin\emptyset + m\ddot{x}_h h\cos\emptyset + M(\emptyset) + c_\emptyset\dot{\emptyset} = 0 \qquad (2.1)$$

where m denotes the mass lumped at the tip of the SDOF pendulum, h is the pendulum's length, $M(\emptyset)$ is the rotational resistance of the spring, P is the vertical load, $\emptyset$ is the deviation of the pendulum from vertical axis, which fully defines location of the mass, and, $\ddot{x}_h$ and $\ddot{x}_v$ are horizontal and vertical base accelerations, respectively. Damping is presented by a rotational dashpot damper with parameter $c_\emptyset$.

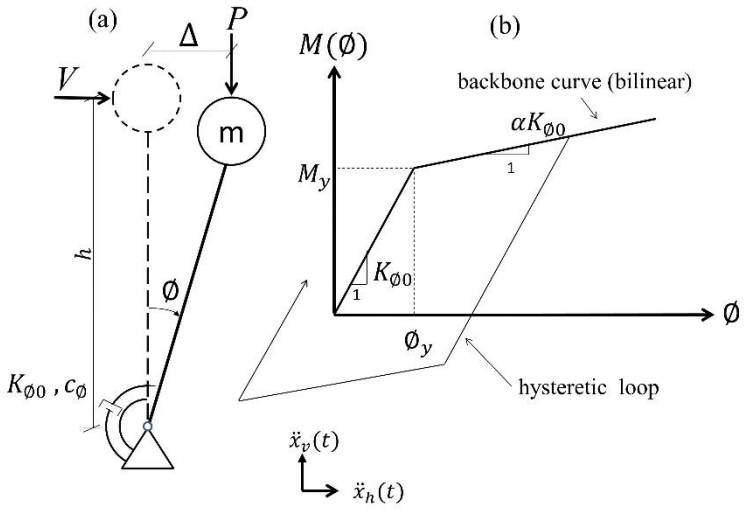

Figure 2.1: The SDOF model subjected to biaxial excitation.

The equation of motion under horizontal excitation can be derived as:

$$mh^2\ddot{Ø} - Ph\sin Ø + m\ddot{x}_h h\cos Ø + M(Ø) + c_Ø\dot{Ø} = 0 \qquad (2.2)$$

To reduce the number of independent parameters, the governing equation of motion might be further simplified. In this regard, the notion of SC is used. The SC stipulates the static stability of the corresponding elastic system subjected to a constant vertical load *P*, and is defined by:

$$\text{SC} = \theta = P/P_{cr} = P.h/K_{Ø0} \qquad (2.3)$$

where, $K_{Ø0}$ is the initial rotational stiffness and $P_{cr} = K_{Ø0}/h$. Substituting Eq.(2.3) into Eqs.(2.1 and 2.2) will read:

$$mh^2\ddot{Ø} - \theta K_{Ø0}(1 + \ddot{x}_v/g\,)\,sin\,Ø + m\ddot{x}_h h\cos Ø + M(Ø) + c_Ø\dot{Ø} = 0 \qquad (2.4)$$

and,

$$mh^2\ddot{Ø} - \theta K_{Ø0}\,sin\,Ø + m\ddot{x}_h h\cos Ø + M(Ø) + c_Ø\dot{Ø} = 0 \qquad (2.5)$$

which are the geometrically nonlinear equations of motion under uniaxial and biaxial excitations, respectively.

Numerical solution of Eqs. (2.4 and 2.5) needs a prior knowledge on the value of θ which in some studies has been taken as constant (Christoph Adam & Jäger, 2012a; Hjelmstad & Williamson, 1998). However, Aydınoğlu and Fahjan (2003) showed that SC itself is a period-dependent parameter and using constant values for it produces "misleading results". They indicated that SC of a pendulum with known height cannot vary arbitrarily. As an alternative approach, they reminded that Eq.(2.3) can be rearranged as:

$$\mathrm{SC} = \theta = (g/h)/\omega_0^2 = \omega_G^2/\omega_0^2 \tag{2.6}$$

in which, $\omega_0^2 = K_{\emptyset 0}/(mh^2)$ is the initial circular frequency of the corresponding geometrically linear equation of motion and $\omega_G^2 = g/h$ is the so-called "geometric frequency".

It follows that, by use of Eq.(2.6), the governing equations of motion under biaxial and uniaxial excitations can be written as:

$$mh^2\ddot{\emptyset} - \omega_G^2(1 + \ddot{x}_v/g)\sin\emptyset + m\ddot{x}_h h\cos\emptyset + M(\emptyset) + c_\emptyset\dot{\emptyset} = 0 \tag{2.7}$$

and,

$$mh^2\ddot{\emptyset} - \omega_G^2\sin\emptyset + m\ddot{x}_h h\cos\emptyset + M(\emptyset) + c_\emptyset\dot{\emptyset} = 0 \tag{2.8}$$

respectively.

2.2 Inelastic Equation of Motion

As mentioned before, $M(\emptyset)$ is the rotational resistance of the spring, which is representative of inelastic constitutive relation. There are a variety of possibilities for selection of constitutive relation, from simple elastoplastic ones to complicated models incorporating cyclic deteriorations (L. F. Ibarra et al., 2005). In this study, a versatile model proposed by Sivaselvan and Reinhorn (2000) will be used. The model itself can be considered to be a version of the original Bouc-Wen model

(Ismail, Ikhouane, & Rodellar, 2009). In those models, a new state variable is defined, which is supposed to govern transition from elastic to inelastic regions (also see (Dobson, Noori, Hou, Dimentberg, & Baber, 1997; L. F. Ibarra et al., 2005) for more information).

As indicated above, a new state variable "z" is defined for modeling hysteresis behavior. To this end, $M(\emptyset)/mh^2$ can be written as:

$$M(\emptyset) = aK_{\emptyset 0}\emptyset + (1-a)K_{\emptyset 0}z \tag{2.9}$$

where a is the ratio of the post-yield to initial stiffness and:

$$\dot{z} = \left\{1 - \left|\frac{z}{\emptyset_y}\right|^n [\beta_1 sign(z\dot{\emptyset}) + \beta_2]\right\}\dot{\emptyset} \tag{2.10}$$

in which: $\emptyset_y$ is the yield rotation, and, n, β_1 and β_2 are parameters controlling shape of the curve.

2.3 Geometrically Linear and Nonlinear Equations of Motion

The secondary objective of present study was defined as evaluation of differences between the geometrically linear and nonlinear equations of motion. In other words, it is desired to evaluate whether the amount of error which is presented by approximating $\sin(\emptyset) \approx \emptyset$ and $\cos(\emptyset) \approx 1$ in the equations of motion is acceptable or not. Starting with Eq. (2.7), the geometrically linear version of equation of motion (see section 2.3) under biaxial excitation might be derived as:

$$mh^2\ddot{\emptyset} - \omega_G^2(1 + \ddot{x}_v/g\,)\emptyset + m\ddot{x}_h h + M(\emptyset) + c_\emptyset\dot{\emptyset} = 0 \tag{2.11}$$

Accordingly, the geometrically linear version of the equation of motion under horizontal excitation, Eq.(2.8), is:

$$mh^2\ddot{\emptyset} - \omega_G^2\emptyset + m\ddot{x}_h h + M(\emptyset) + c_\emptyset\dot{\emptyset} = 0 \tag{2.12}$$

In the next chapter a relatively comprehensive evaluation of the effects of neglecting the geometric nonlinearity in estimating the maximum-inelastic-response, and subsequently, the ductility demand of SDOF systems under horizontal excitation is presented.

Chapter 3

EFFECT OF GEOMETRIC NONLINEARITY AT GLOBAL LEVEL ON THE DUCTILITY DEMAND OF SDOF SYSTEMS

3.1 Introduction

Present study tries to systematically evaluate effects of incorporating geometric nonlinearity into the equation of motion, and demonstrate the differences between linear and nonlinear formulations. Using the geometrically nonlinear formulation becomes especially important when large displacements are expected; or, calculating maximum-inelastic-displacements (rotations) are aimed. As mentioned earlier, derivation of an alternative response spectrum and evaluation of the effect of VCGM on the maximum-inelastic-response of SDOFs are the major aims of present study. In both cases, the underlying assumption permitting linearization is violated. Therefore it is desired to investigate whether the use of geometrically linearized version of equation of motion is acceptable or not.

3.2 Objectives and Methodology

To compare the effect of geometric nonlinearity just horizontal excitation is considered. Moreover, the period-dependent feature of SC is neglected since the aim is to compare two formulations under same conditions; while the difference is solely the presence or absence of the geometric nonlinearity. The geometrically nonlinear equation of motion under uniaxial excitation is:

$$mh^2\ddot{\emptyset} - \theta K_{\emptyset 0} \sin\emptyset + m\ddot{x}_h h\cos\emptyset + M(\emptyset) + c_\emptyset\dot{\emptyset} = 0 \tag{3.1}$$

which is same as Eq.(2.5), that is repeated here for convenience. The geometrically linear version of Eq.(3.1) can be derived as:

$$mh^2\ddot{\emptyset} - \theta K_{\emptyset 0}\emptyset + m\ddot{x}_h h + M(\emptyset) + c_\emptyset\dot{\emptyset} = 0 \tag{3.2}$$

Different cases are categorized based on relative values of SC and material hardening. In particular, two major cases depending on whether stability coefficient is equal to or greater than the hardening are investigated. It is worth noting that if nonlinear formulation is used equality of mentioned parameters will result in a special case in which the stiffness apparent in the system will be driven by nonlinear terms of the rotation angle. To show this, it is noted that the apparent stiffness of the system in a geometrically linear system (see section 2.3) is given by:

$$M(s)_{Linear} = M(\emptyset) - \theta K_{\emptyset 0}\emptyset \tag{3.3}$$

while that of a geometrically nonlinear formulation might be approximated as:

$$M(s)_{non-linear} = M(\emptyset) - \theta K_{\emptyset 0}\emptyset + \theta K_{\emptyset 0}\frac{\emptyset^3}{3!} - m\ddot{x}_h h\frac{\emptyset^2}{2!} \tag{3.4}$$

in which:

$$\sin\emptyset \approx \emptyset - \frac{\emptyset^3}{3!} \tag{3.5}$$

and,

$$\cos\emptyset \approx 1 - \frac{\emptyset^2}{2!} \tag{3.6}$$

are used. Now if $a = \theta$, then by use of Eq.(2.9) one has:

$$M(s)_{Linear} = (1-\theta)K_{\emptyset 0} z \tag{3.7}$$

while for a geometrically nonlinear formulation one has:

$$M(s)_{non-linear} = (1-\theta)K_{\emptyset 0} z + \theta K_{\emptyset 0}\frac{\emptyset^3}{3!} - m\ddot{x}_h h\frac{\emptyset^2}{2!} \tag{3.8}$$

It can be seen that for large responses, i.e. at or near the collapse stage, nonlinear terms of the rotation and characteristics of the forcing function will also affect the response of geometrically nonlinear systems.

Both harmonic excitations, with different levels of amplitudes and frequencies, and the FEMA p-695 set of recorded motions are used in analysis (Foschaar, Baker, & Deierlein, 2012). For harmonic excitations, a sinusoidal excitation introduced as:

$$\frac{\ddot{x}_h(t)}{g} = \nu \ \sin(\Omega t) \tag{3.9}$$

is substituted into Eqs.(3.1 and 3.2). Although harmonic excitations do not perfectly resemble the earthquakes, their constant frequency and amplitude may highlight influential parameters, which may remain hidden otherwise. For instance, in light of Eq.(3.9), the effect of excitation characteristics on the apparent resistance of a geometrically nonlinear system, Eq.(3.8), becomes clearer.

The ductility demand predicted by geometrically linear and nonlinear formulations are compared for systems with different levels of relative strengths (R-factor). When the SC is equal to hardening, significant differences in calculated ductility demands were observed. If SC is larger than hardening, differences are manifested in terms of stability. While linear approximation shows unstable response, the response of the nonlinear formulation remains stable. Stability of the solution of the nonlinear formulation might enhance computational performance when investigating full range behavior of a system is desired. For instance, such a situation might be encountered during collapse evaluation.

A bilinear hysteresis relation with positive hardening defines the spring behavior for all cases. Using different hysteresis relations is not within the scope of present study. This is mainly because previous literature indicates that the necessary increase in strength to maintain same ductility level in presence and absence of P-delta effect is larger for SDOFs with bilinear hysteric behavior. However, it is worth noting that any other hysteric behavior should be incorporated simultaneously into both formulations; and thus, results are expected to change in the same manner.

When SC is equal to hardening, ductility-demands are calculated based on linear and nonlinear formulations, and are compared through a percentage difference defined as:

$$Difference = \left|\frac{\mu_{non} - \mu_{lin}}{\mu_{non}}\right| \times 100 \qquad (3.10)$$

where "μ_{non}" and "μ_{lin}" represent ductility demands predicted by nonlinear and linear formulations, respectively. For the sake of consistency, in all calculations maximum elastic rotations are also computed based on linear and nonlinear formulations. In other words, maximum elastic rotations used in inelastic-nonlinear and inelastic-linear demand calculations are based on, elastic-nonlinear and elastic-linear formulations, respectively. Elastic linear and elastic nonlinear equations can be derived by substituting $M(\emptyset) = K_{\emptyset 0}\emptyset$ into Eqs.(3.1 and 3.2). Yield rotations can be established by dividing maximum elastic rotations by the R-factor.

Sinusoidal excitations with three levels of amplitude (0.15, 0.3 and 0.45g), and five levels of frequency (5, 10, 15, 20 and 25 rad/s) are chosen as harmonic excitations. All harmonic excitations are applied for 30 seconds followed by 10 seconds of free vibration (Hjelmstad & Williamson, 1998).

For values of hardening less than SC, two records, namely: El-Centro and Northridge, are used. Systems with four different levels of relative strengths (R-factor) are studied. Damping ratio in all cases is kept at 5%.

An established routine in earthquake engineering is to plot changes of a parameter in consideration versus system's initial period. Here, the percentage of difference between ductility demands calculated by either formulations, as defined in Eq. (3.10), is plotted against the system's initial period. Those plots are referred to as percentage of difference versus period (PD-T) graphs, here after.

3.3 Stability Coefficient Equal to Hardening

3.3.1 Harmonic Excitations

Obviously it is not plausible to consider all pairs which satisfy the condition $a = \theta$. Therefore, results are presented for a 5% damped system with $a = 0.05$ and $\theta = 0.05$.

Figure 3.1 shows the PD-T graphs under action of a sinusoidal excitation with an amplitude of ν = 0.3g and a frequency of Ω =10 rad/s for four levels of relative strengths. As can be seen, in short period range the level of relative strength has significant effect on the differences between the two formulations. The absolute value of the difference exceeds 100% for R-factors equal to 4, 6 and 8. On the other hand, by increasing the relative strength the range of periods that are sensitive to geometric nonlinearity expands.

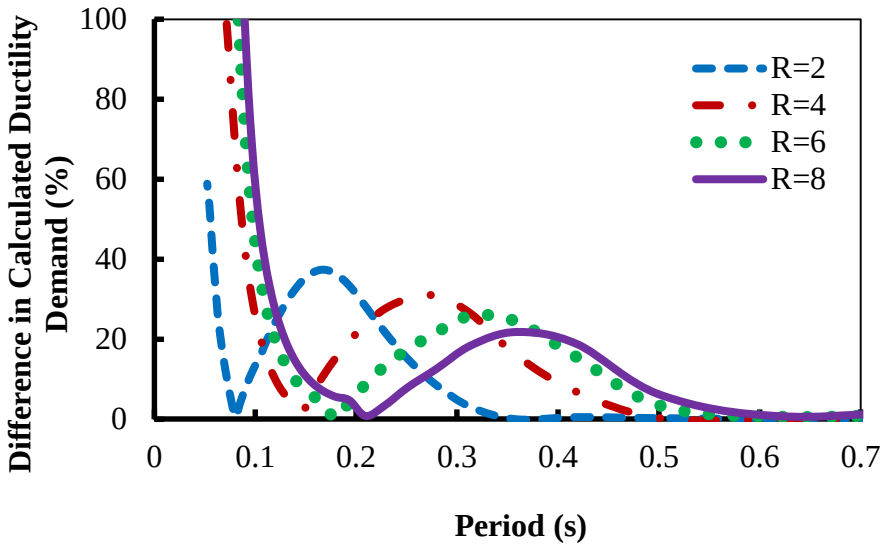

Figure 3.1: PD-T diagrams for four levels of reduction factor (R=2, 4, 6 and 8) under a sinusoidal excitation with amplitude of 0.3g and frequency of 10(rad/s). a = 0.05, θ = 0.05 and ζ = 0.05.

Same phenomenon can be seen in Figure 3.2. In that Figure, instead of the percentage of difference, the ductility demand calculated by geometrically nonlinear formulation is normalized to the ductility demand calculated by geometrically linear formulation. For all levels of relative strength, geometrically linear approximation significantly overestimates the ductility demand at short period region. A marginal underestimation is noticeable for periods in the range of 0.2 to 0.4s. Hence, the geometrically linear formulation is not always conservative and may introduce bias in predicting the maximum-inelastic-responses.

The difference between calculated ductility demands is very sensitive to the frequency of excitation, as can be seen in Figure 3.3.

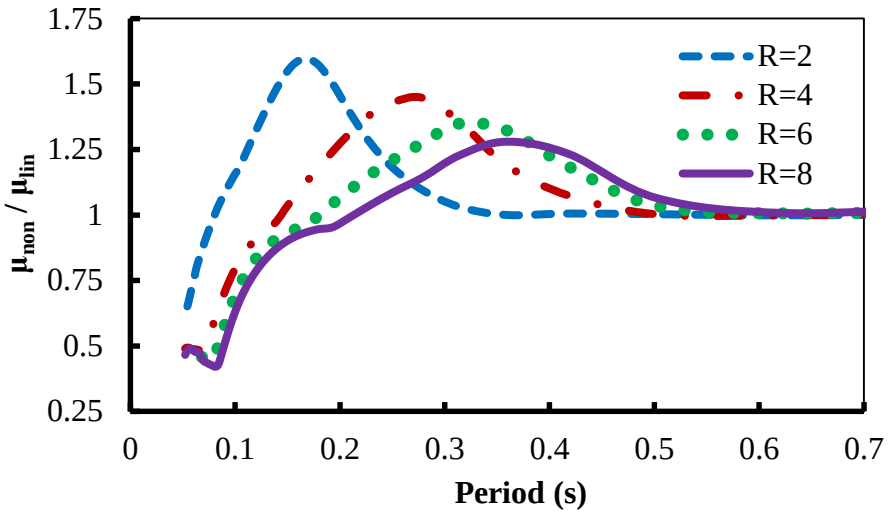

Figure 3.2: Ductility demand predicted by nonlinear formulation normalized by linear one for four levels of relative strength (R=2, 4, 6 and 8). Amplitude of excitation is 0.30g and its frequency is 10 (rad/s). a = 0.05, θ = 0.05 and ζ = 0.05.

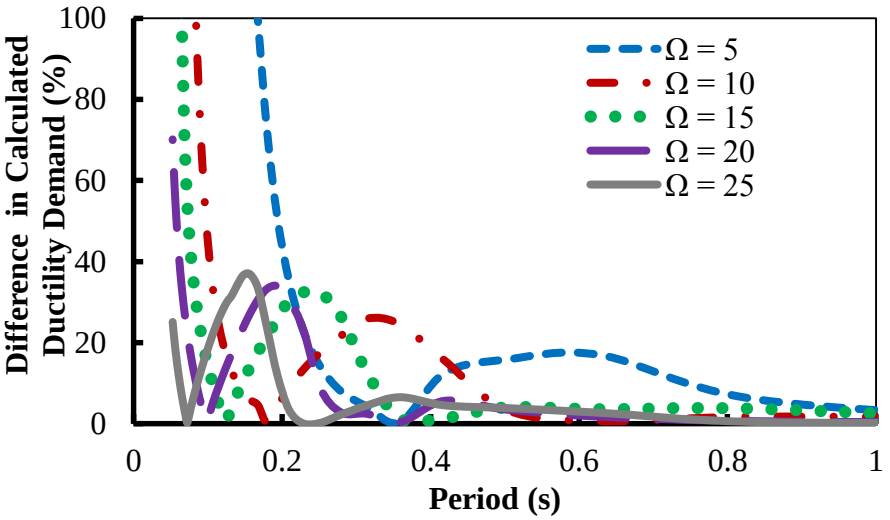

Figure 3.3: Effect of frequency of excitation on PD-T for five different levels of frequencies. Amplitude of excitation is 0.3g, R=6, a = 0.05, θ = 0.05 and ζ = 0.05.

It is also worth noting that the effects of the frequency of excitation and relative strength are similar in the sense that a larger R-factor has the same effect as a lower frequency of excitation (compare with Figure 3.1).

An increase in the amplitude of excitation results in an increase in the difference in predicted ductility demand, as can be seen in Figure 3.4. However, and unlike R-

factor or the excitation's frequency, variations of the amplitude does not change the range of periods that are sensitive to the geometric nonlinearity.

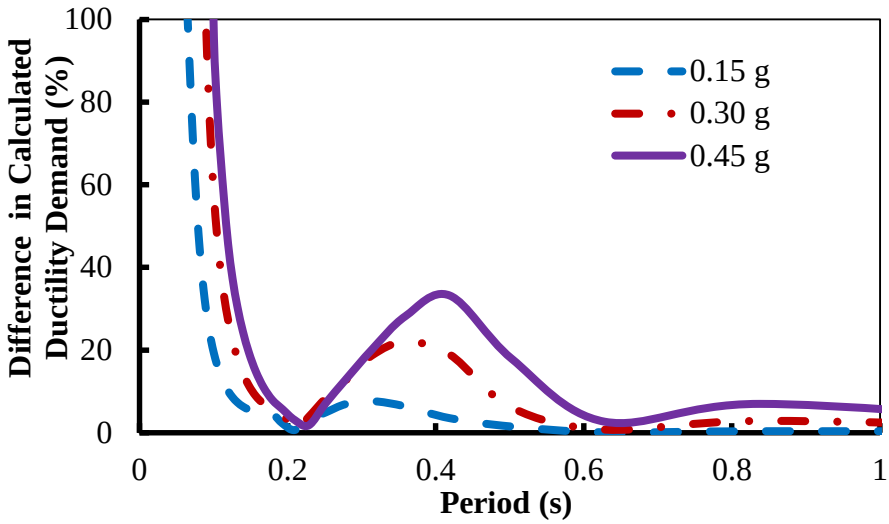

Figure 3.4: Effect of amplitude of excitation on PD-T diagram for three levels of amplitudes. a = 0.05, θ = 0.05 and ζ = 0.05.

3.3.2 Real Earthquake Records

As stated earlier, harmonic excitations, with constant frequency and amplitude, do not perfectly resemble real earthquakes. Therefore, it might be interesting to examine effect of geometric nonlinearity under action of real ground motion records.

Figure 3.5 shows the PD-T graph for a system with R=8 subjected to the FEAM p - 695 set of recorded motions. Results show that the differences reach up to 100% and more in the short period range. Note that differences more than 100% are omitted, although values well beyond 100% were observed.

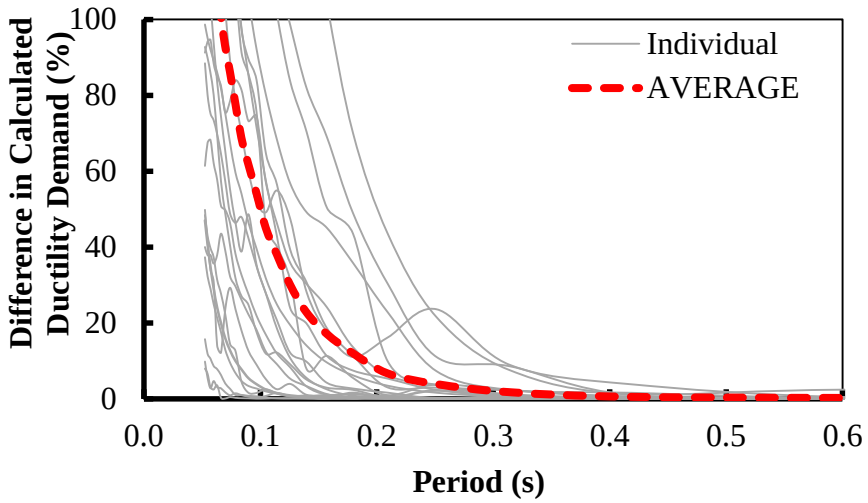

Figure 3.5: PD-T diagram for FEMA P-695 set of recorded motions for a system with R=8.

The difference between linear and nonlinear formulation at short period range is especially important since the well-known equal displacement rule is not applicable in that region (Miranda, 2000).

Many researchers have tried to approximate maximum-inelastic-displacements based on maximum-elastic ones by using various SDOF systems (Miranda & Ruiz-García, 2002). However, to the best of the authors' knowledge, P-delta effect has not been considered for systems without NPYS. Therefore, present study becomes especially important since it shows that by including the P-delta effect maximum difference between linear and nonlinear formulations is expected in the same region. In particular, results of present study might be considered in line with results of Ruiz-Garcia and Miranda (Ruiz-García & Miranda, 2003), since the difference between geometrically linear and nonlinear formulations in the case of equal SC and material hardening is equivalent to a difference between a system experiencing positive-post-yield-stiffness (PPYS) and an elasto-plastic one. However, it is worth noting that PPYS in present study arises from consideration of the P-delta effect and higher

order terms of generalized coordinate system, while in the mentioned study material hardening was the source of PPYS.

The mean differences for four levels of the relative strength and under action of the FEAM p-695 set of recorded motions are shown in Figure 3.6. It can be seen that increasing the relative strength will expand the range of sensitive periods, and hence, is in line with results obtained by use of harmonic excitations.

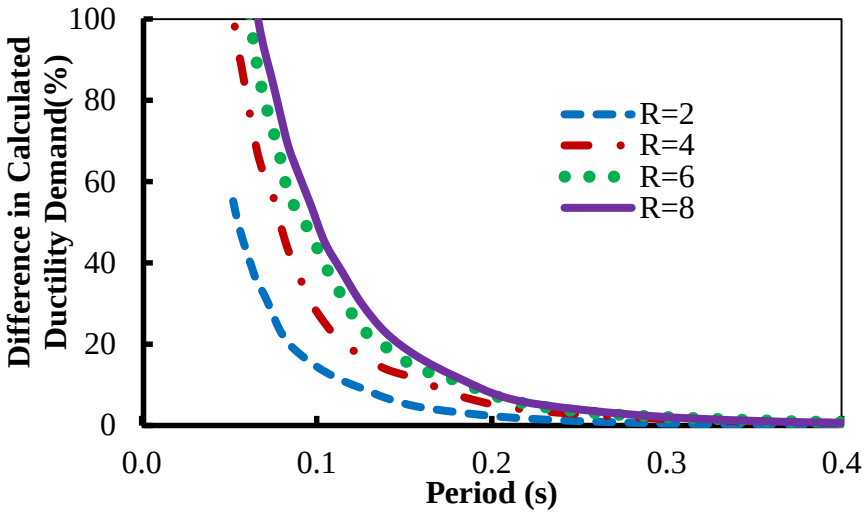

Figure 3.6: Mean PD-T for FEMA P-695 set of recorded motions for four levels of R (R=2, 4, 6 and 8).

Effect of scaling a record is shown in Figure 3.7, where differences of the calculated ductility demands by use of the original record are compared to those calculated under four various scales of it. It can be seen that the results are quite comparable to those obtained by use of harmonic excitations; that is, scaling a record will intensify the difference between the calculated ductility demands, without changing the range of sensitive periods.

Based on the presented results, it can be concluded that in short period range significant differences in predicted ductility demands by use of either geometrically linear or nonlinear formulations is expected. As a result, neglecting geometric nonlinearity may introduce bias in calculating the maximum-inelastic-displacements.

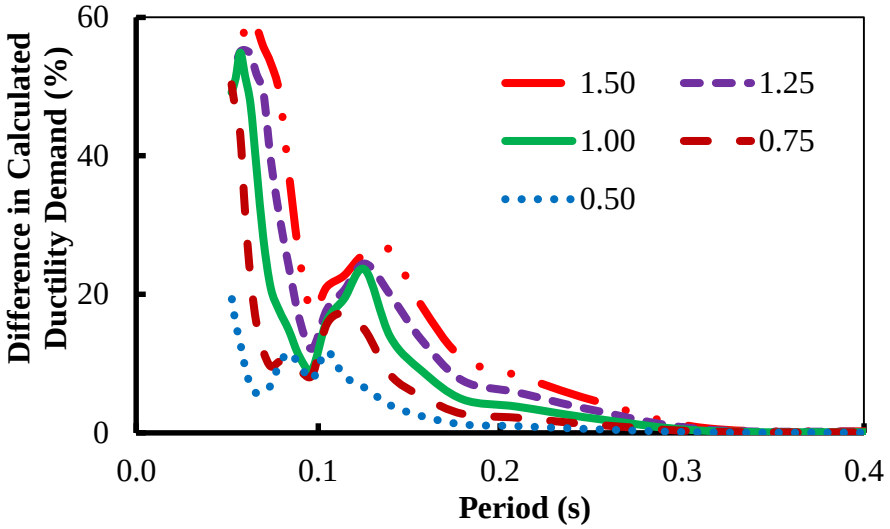

Figure 3.7: PD-T diagram for an individual record scaled to five levels of PGA; PGA=1 corresponds to original record.

3.4 Stability Coefficient Greater Than Hardening

Because of devastating economic and social consequences, earthquake-engineering codes intend to keep the probability of structural collapse endurably low such that public safety is assured (C. B. Haselton & Deierlein, 2008; Liel, Haselton, Deierlein, & Baker, 2009; Shi, Lu, Guan, & Ye, 2014). This, however, needs a precise knowledge on the state of a structure from elastic to inelastic, and finally, to the collapse stage.

Previous studies have mentioned two modes of failure, namely: sidesway collapse and vertical collapse, as the most commonly observed ones (Zareian, Krawinkler, Ibarra, & Lignos, 2010). Vertical collapse identifies direct loss of vertical load

carrying capacity. On the other hand, sidesway collapse is a result of shearing of lateral strength due to excessive deformations under a strong ground motion, which will result in strength and stiffness deteriorations, and consequently, will cause total or partial loss of load-carrying capacity in a building structure (C Adam & Ibarra, 2015; Jäger & Adam, 2013). The latter, sometimes referred to as global P-delta effect, may lead to development of NPYS, even though structural elements may not necessarily experience deterioration. For instance, ASCE indicates that if a single element passes a pre-specified threshold, usually defined in terms of plastic rotations, collapse state has reached. Some studies have reminded that such a definition is conservative and identifies "near-collapse" state, since a given structure will not necessarily become unstable in that condition (C. B. Haselton, Liel, & Deierlein, 2009). Hence, element failure and global instability need to be distinguished. It follows that unstable state of a structure may reach at or beyond the collapse threshold, as indicated by Jäger and Adam (2013). This issue may justify using the geometrically nonlinear formulation.

3.4.1 Harmonic Excitations

If $a < \theta$, then the system shows NPYS and under sufficiently strong excitation is expected to exhibit dynamic instability. It is desired to investigate effect of higher order terms (geometric nonlinearity) on behavior of such systems at or near collapse stage.

In literature there are several definitions for collapse (Haselton, Liel, & Deierlein, 2009). Some scholars have used the "actual collapse" based on backbone of the force-deformation relation. On the other hand, some researchers have used the Lyapunov's criteria. "Roughly, it states that the motion of a structure is stable if any

possible small change in the initial condition can lead only to a small change in the response" (Bažant, 2000). In the present work, both mentioned definitions would be used for identification of collapse.

Consider a 5% damped system with $a = 0.04$, $\theta = 0.05$, R=8, and an initial period of 0.15s, under a sinusoidal excitation with a frequency of Ω =20 (rad/s) and an amplitude of ν = 0.3g. Velocity versus rotation diagrams (the phase-portrait) of this system for geometrically linear and nonlinear systems are presented in Figure 3.8. It can be seen that linearly formulated system shows unbounded response while nonlinear formulation returns to a stable position.

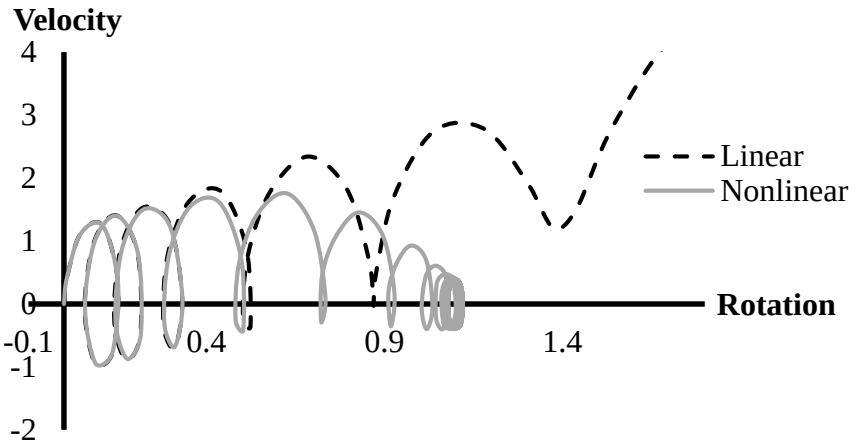

Figure 3.8: Velocity-rotation diagram for nonlinear (continuous) and linear (dashed) formulations under sinusoidal excitation with amplitude of 0.3g and frequency of 20(rad/s). R=8, T=0.15s, a = 0.04, θ = 0.05.

The same phenomenon can be seen based on lateral resistance of the system in Figure 3.9. Effect of higher order terms can be seen in that figure; that is, while resistance of geometrically linear system drops to zero, the geometrically nonlinear system still shows resistance.

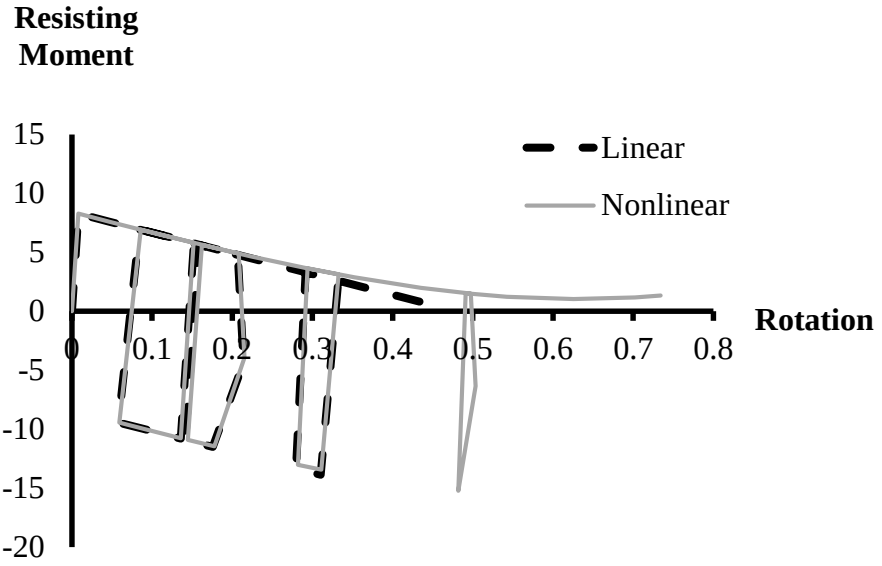

Figure 3.9: Resisting moment-rotation diagram for nonlinear (continuous) and linear (dashed) formulations under sinusoidal excitation with amplitude of 0.3g and frequency of 20(rad/s). R=8, T=0.15s, a = 0.04, θ = 0.05.

Advantage of geometrically nonlinear formulation is in mathematical stability of the solution, which helps to overcome convergence problems. When full range behavior of a system, from elastic to collapse, is investigated, numerical stability of the solution could be greatly enhanced by use of geometrically nonlinear formulation.

Effect of variations of the excitation's characteristics on the estimated ductility demands by either formulation is demonstrated through normalized ductility demand. Consider 5% damped systems with initial periods ranging from 0.05 to 1.25s subjected to a sinusoidal excitation with an amplitude of ν = 0.3g. Other parameters are kept same as in the previous example. Five levels of excitation frequencies were examined; however, just three of them are presented in Figure 3.10. This is because zero ratios were observed for the other two frequencies on the whole range of the examined periods. Note that a zero ratio identifies unbounded response of the geometrically linear formulation. This conclusion is possible since nonlinear

formulation showed stable response for the whole range. Figure 3.10 can also be used to identify regions of numerical stability of linear equation of motion.

Two important issues could be identified based on that Figure. First, except for a limited range of periods, the difference between two formulations in calculating the ductility demands is very large; i.e., zero ratios were observed for majority of periods. Second, for each specific excitation's frequency, a non-zero ratio corresponds to stability of linear equation of motion. Thus, it can be seen that by increasing the frequency of excitation the regions where the response is stable shifts towards shorter periods.

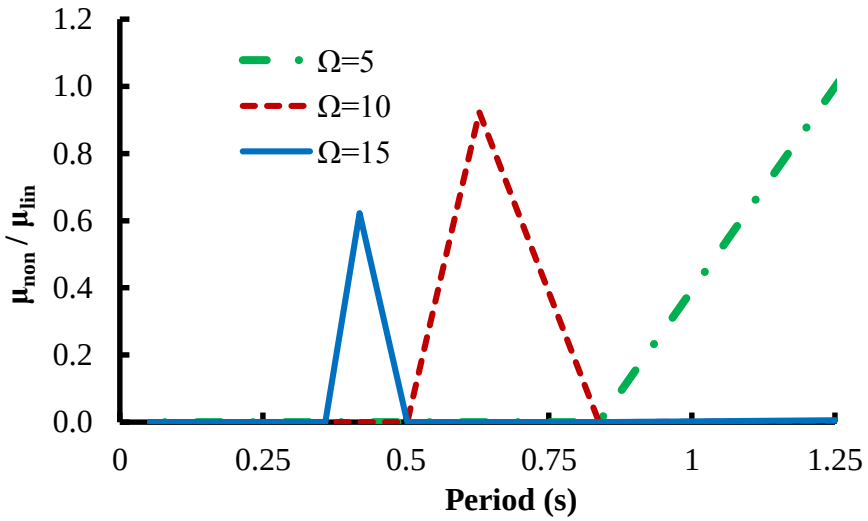

Figure 3.10: Effect of frequency of excitation on ductility demand predicted by nonlinear formulation normalized by linear one for three different frequencies. Excitation amplitude is 0.3g, R=8, a = 0.04, θ = 0.05 and ζ = 0.05.

Effect of the amplitude of excitation on the response can also be studied based on the ratio of the ductility demands predicted by each formulation. For example, Figure 3.11 plots the ratio of the ductility demands predicted by either geometrically linear and nonlinear formulations for 5% damped systems subjected to a sinusoidal excitation with a frequency of Ω =10 (rad/s) and for three levels of amplitudes. It can

be seen that the regions where the response of the geometrically linear system is stable does not change by changing the amplitude of excitation. However, the difference in calculated ductility demands is intensified by increasing the amplitude of excitation.

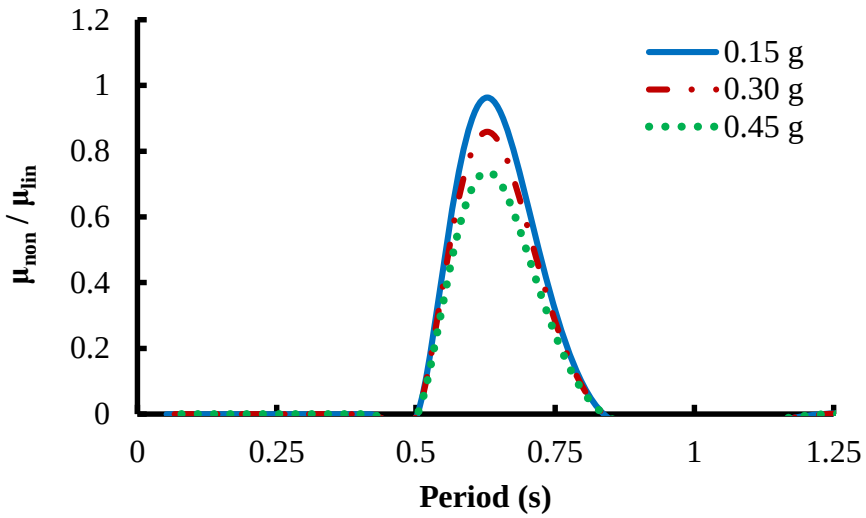

Figure 3.11: Effect of amplitude of excitation on ductility demand predicted by nonlinear formulation normalized by linear one for three different amplitudes. Excitation frequency is 10 (rad/s), R=8, a = 0.04, θ = 0.05 and ζ = 0.05.

The effect of variations of the strength reduction factor on the predicted ductility demands by either formulations is plotted in Figure 3.12. It can be seen that the range of initial periods corresponding to stable response of the geometrically linear systems decreases by increasing the R-factor. Thus, consideration of the geometric nonlinearity is specifically important for flexible structures.

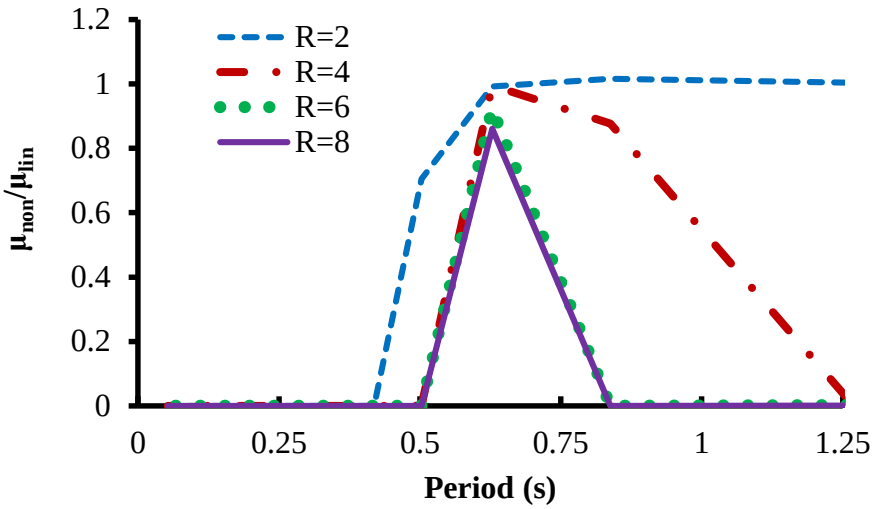

Figure 3.12: Ductility demand predicted by nonlinear formulation normalized by linear one for four levels of reduction factor (R=2, 4, 6 and 8). Amplitude of excitation is 0.30g, angular frequency is 10 (rad/s), a = 0.04, θ = 0.05 *and* ζ = 0.05.

3.4.2 Real Earthquake Records

Results under action of real ground motion records are essentially the same as the harmonic excitation cases. Specifically, geometrically linear systems lose their stability, while geometrically nonlinear systems remain stable. When applying response history analysis (RHA), numerical instability of the geometrically linear formulation forced the analysis to stop in some cases. However, numerical stability of the geometrically nonlinear formulation permitted the analysis to finish in all cases. This indicates the reliability of the latter formulation in revealing the behavior of a system well beyond its elastic limit.

To show the difference between the two formulations two classic records, namely, the El-Centro and Northridge records are chosen.

Consider a 5% damped system with an initial period of 0.35s, a hardening of $a = 0.04$, an SC of $\theta = 0.05$, a reduction factor of R=8, subjected to El-Centro and Northridge ground motions. Velocity versus rotation, and resisting moment versus

rotation diagrams, are shown in Figures 3.13 and 3.14, for El-Centro record, and in Figures 3.15 and 3.16 for Northridge record, respectively.

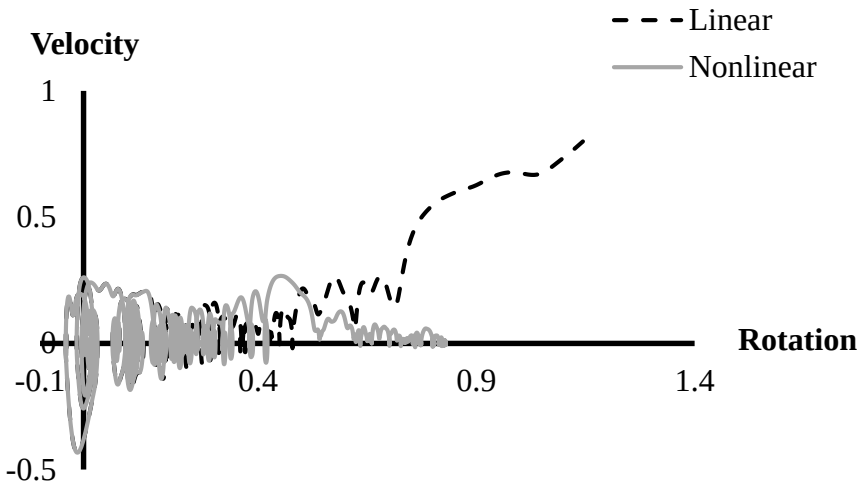

Figure 3.13: Velocity versus rotation (Phase) diagram for a 5% damped system with reduction factor of R=8 and initial period of 0.35s, subjected to El-Centro ground motion. a = 0.04, θ = 0.05.

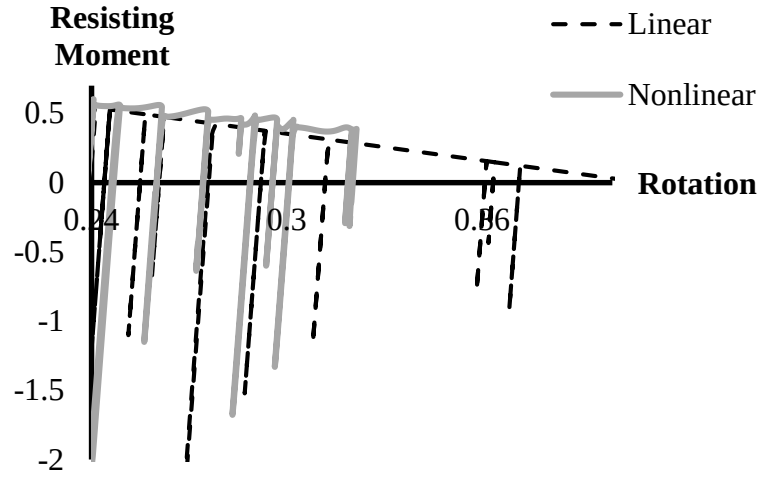

Figure 3.14: Resisting moment versus rotation of a 5% damped system at near collapse stage with reduction factor of R=8 and initial period of 0.35s, subjected to El-Centro ground motion. a = 0.04, θ = 0.05.

It is worth noting that in plotting the resisting moment versus rotation graphs the near collapse stage is demonstrated for the sake of a more clear presentation. Also, note

that the two formulations are not necessarily at the same stage of a RHA. This is due to numerical instability of the geometrically linear formulation.

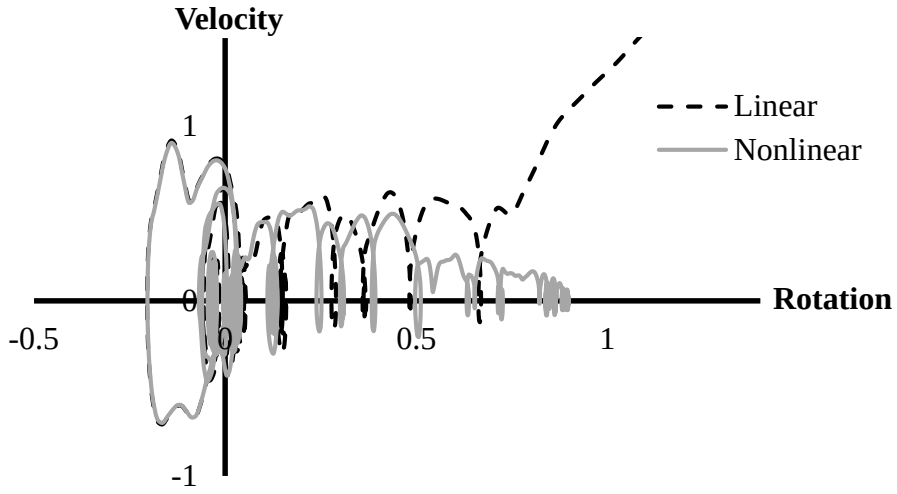

Figure 3.15: Velocity versus rotation diagram for a 5% damped system with reduction factor of R=8 and initial period of 0.35s, subjected to Northridge ground motion. a = 0.04, θ = 0.05.

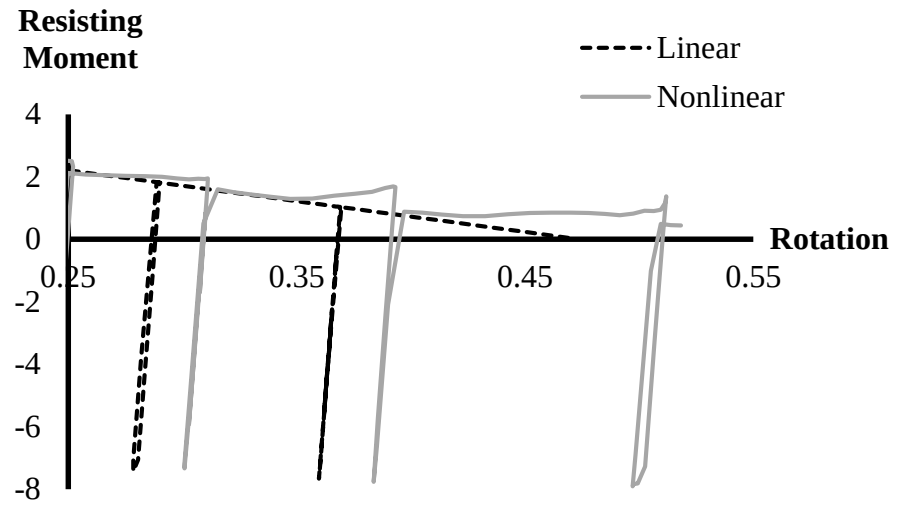

Figure 3.16: Resisting moment versus rotation of a 5% damped system at near collapse stage with reduction factor of R=8 and initial period of 0.2s, subjected to Northridge ground motion. a = 0.04, θ = 0.05.

For the both mentioned recorded motions, linear system reaches to a state of dynamic instability faster, and in earlier stages of analysis. On the other hand, nonlinear system shows resistance even when linear system has collapsed. This phenomenon

introduces bias in predicting collapse point. Moreover, monitoring behavior of the system from elastic to inelastic, and eventually to dynamic instability or up to high rotations, is more reliably carried out should the nonlinear formulation is adopted. This may overcome some convergence problems and enhance computational procedure.

Chapter 4

THE FIRST STOREY SINGLE DEGREE OF FREEDOM SYSTEM AND THE STABILITY COEFFICIENT RESPONSE SPECTRA

4.1 Introduction

Among various problems, structural designers are faced with two important issues at early stages of a design project. The first one is how to select preliminary dimensions for structural elements. The second one is how to reduce the number of necessary iterations during design process.

As stated earlier, reflection of previous studies on seismic codes is a combination of previously proposed strategies. For example, according to Eurocode 8, ASCE7-10, and Turkish Standards (TEC, 2018), P-delta effect can be neglected if SC is sufficiently small. To neglect P-delta effect, Eurocode 8 and ASCE7-10 demand for SC to be less than 0.1, while Turkish Standards' limit is 0.12. The first two specifications allow counterbalancing the P-delta effect by amplifying lateral forces/displacements if SC is larger than 0.1, but less than 0.25 in ASCE7-10, and 0.3 in Eurocode 8, respectively. If the SC is larger than the above-mentioned limits lateral stiffness of the structure should be adjusted to bring it to one of the previous conditions.

Two important issues are worth highlighting here. First, satisfying code specified limits regarding SC demands for several trials; that is, after increasing lateral stiffness, fundamental period of vibration will change and hence a new set of lateral forces should be calculated. In addition, since restrictions on SC are not directly imposed on the fundamental period of vibration, a design project may potentially start with any preliminary selection. Therefore, a reliable starting point may enhance the overall procedure. In this respect, some studies focused on derivation of the minimum necessary lateral stiffness, or the critical strength reduction factor, that prevents dynamic instability (Bernal, 1992, 1998; Miranda & Akkar, 2003). For instance, Christoph Adam and Jäger (2012a) developed the so-called collapse-capacity-spectra for SDOF systems, with various levels of SC and hysteresis behavior (also see (Christoph Adam & Jäger, 2012b). Although such limits might indirectly be used as a design aid, since those methods are mainly assessment oriented, the presented limits are rarely practical in satisfying SC restrictions at early stages.

Second, reliable inclusion of P-delta effect in construction of nonlinear constant-ductility-response-spectrum is a vital step in both SBD and DBD methods. Explicitly, derivation of dependable amplification factors demands for construction of a reliable response spectrum including P-delta effect in first place. While some of previous studies had used constant values for SC (Bernal, 1987), Aydınoğlu and Fahjan (2003) showed that SC itself is a period-dependent parameter and treating it as a constant value produces “misleading results”. They argued that for developing any period-dependent spectrum, for consistency, period-dependence of SC should be considered. To achieve a consistent treatment of P-delta effect, they reformulated the recursive solution procedure of linear SDOF systems in a unified format to address

response of nonlinear SDOF systems with multi-linear hysteresis behavior. The unified-piece-wise-exact-method (UPEM) utilizes the so-called "geometric frequency" which reflects the period-dependence nature of SC. Importance of the period-dependence feature of SC was also indicated by Kalkan and Graizer (2007) who mentioned that: in derivation of response spectrum of P-delta affected systems period cannot serve as a convenient measure unless the pendulum's height is kept constant. Using constant height is equivalent to adaptation of period-dependent SC, which is an important feature of the UPEM. Nevertheless, the method has not been extended to MDOFs.

The fundamental idea behind the first-storey-single-degree-of-freedom (FSSDOF) system is to overcome the mentioned problems by setting a reasonable starting point. In other words, the FSSDOF system is aimed to set a reasonable minimum requirement on the necessary lateral stiffness of a structure, by trying to satisfy code specified limits regarding the SC and inter-storey drifts at early stages.

4.2 Pendulum Based Response Spectra

In its most general form a response spectrum is a plot of spectral information against dynamic properties of a SDOF system. Conventionally, fundamental period of vibration has been adopted for construction of the response spectra. As stated earlier, for presenting P-delta effect, fundamental period cannot serve as a convenient measure unless the pendulum's height is kept constant. As an example, constant ductility response spectra for a 3.0m long inverted-pendulum model (with P-delta), and its corresponding MSD model (without P-delta), are compared in Figure 4.1. Bilinear material behavior with 5% hardening and 5% damping are considered. In

construction of Figure 4.1 *Kocaeli* earthquake (1999, Turkey), recorded at *Yarimca*, is used as the input motion.

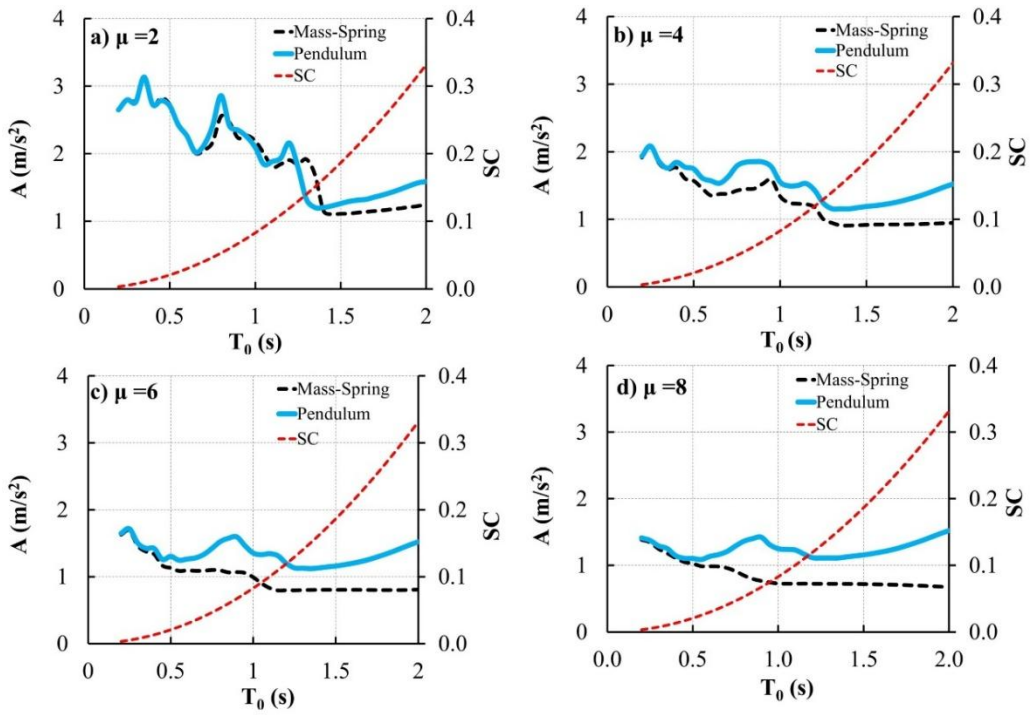

Figure 4.1: Comparing constant ductility response spectra of inverted-pendulum model (with P-delta), and its corresponding mass-spring-damper model (without P-delta), for various levels of ductility. *Kocaeli* earthquake, recorded at *Yarimca*, is used as input motion.

It is worth noting that the horizontal axis in Figure 4.1 represents the pendulum's initial period T_0, which is given by:

$$T_0 = \frac{2\pi}{\omega_0^2} \tag{4.1}$$

Consequently, it is logical that the divergence between the mentioned spectra increases with increasing period (owing to the period-dependent feature of SC). However, and as stated earlier, seismic resistance codes demand for the SC to be limited to certain thresholds. This is equivalent to imposing an upper limit on the pendulum's period (see Eq. (4.2)). For the above-mentioned example, with $\omega_G^2 = 3.27\ \mathrm{rad/s^2}$, the maximum permissible period according to Turkish standards (SC =

0.12), ASCE 7-10 (SC = 0.25), and Eurocode 8 (SC = 0.3), can be calculated as 1.20, 1.74, and 1.90s, respectively. The lateral stiffness of any system with a longer period should be increased to bring it to one of the mentioned regions. Therefore, for the presented example analysis is followed up to T_0 = 2.0s.

Some important features of Figure 4.1 are worth mentioning at this stage:

- Regardless of the level of ductility, P-delta effect is negligible for short period systems. As discussed earlier, this observation is in agreement with the previous studies and code specifications.
- For systems with longer periods, and for all levels of ductility, the spectral acceleration calculated by the pendulum model remains unchanged.
- The divergence between the two spectra becomes more noticeable by increasing the level of ductility.

It might be interesting to investigate the effectiveness of the code specified amplification factors and suitability of the SC below which the P-delta effect is deemed negligible based on the inverted pendulum model.

Figure 4.1 shows that except for μ = 2 all the above-mentioned codes overestimate the SC below which P-delta effect is trivial. In other words, limiting the SC to a value less than 0.1 may not necessarily result in negligible P-delta effect. This might be attributed to the fact that ignoring the period-dependent feature of SC causes a systematic underestimation of the P-delta effect by increasing period. The mentioned phenomenon seems to be more noticeable for highly ductile systems. Likewise, using

the amplification factors may not completely counterbalance the P-delta effect for the same reason. This might be better viewed in Figure 4.2.

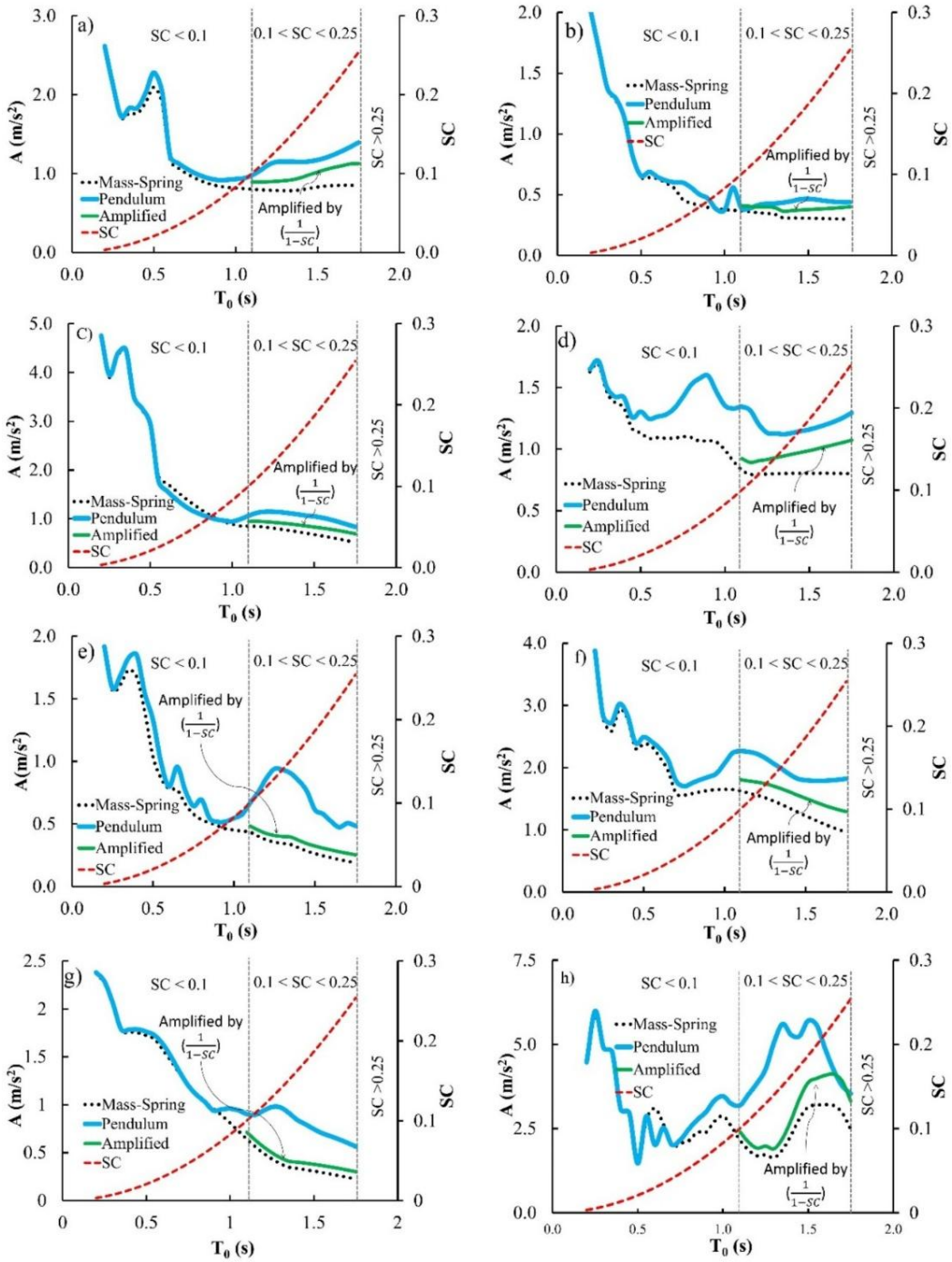

Figure 4.2: Constant-ductility-response-spectrum (μ = 6) based on pendulum model (with P-delta), mass-spring model (without P-delta), and amplified version of mass-spring model per ASCE7-10. Regions of negligible P-delta, and where P-delta is allowed to be counterbalanced with amplification factors are indicated. a) Imperial Valley-06, b) Landers, c) Kobe, d) Kocaeli, e) Duzce, f) Bam, g) Parkfield, and h) Darfield.

In Figure 4.2, suitability of the amplification factors for counterbalancing the P-delta effect is assessed on a set of records that are presented in Table 4.1 (Downloaded at PEER-NGA2 Ground Motion Database (https://ngawest2.berkeley.edu/)). The presented set of ground motions consists of strike-slip earthquakes recorded at near fault. The regions of negligible P-delta effect, where it is allowed to be counterbalanced, and where according to ASCE 7-10 specifications the system's lateral stiffness should be increased are also illustrated. In addition, and based on the amplification factors defined in the mentioned code $(1/(1-SC))$, the amplified version of the MSD's spectrum is shown in the relevant region of periods. Figure 4.2 indicates that the amplified MSD's spectrum noticeably underestimates the P-delta effect for all the examined records. Notably, Amara et al. (2014) concluded the same results although they used constant SC.

Table 4.1: The set of recorded motions used in Figure 4.2.

Earthquake	**Year**	**Station**	**Magnitude**	**Component**	**PGA (*g*)**
Imperial Valley-06	1979	El Centro Array #5	6.53	E05140	0.53
Landers	1992	Lucerne	7.28	LCN345	0.79
Kobe	1995	Takarazoka	6.90	TAZ090	0.61
Kocaeli	1999	Yarimca	7.51	YPT060	0.23
Duzce	1999	IRIGM 487	7.14	487-EW	0.28
Bam	2003	Bam	6.60	BAM-T	0.63
Parkfield-02-CA	2004	Parkfield - Cholame 1E	6.00	C01090	0.44
Darfield	2010	GDLC	7.00	GDLCN5W	0.76

Obviously, upon selection of a suitable set of recorded motions, it is possible to construct an alternative design spectrum based on the pendulum model. Having said this, in the current state-of-practice record selection and scaling strategies are based on MSD models. Hence, suitability of such methods when applied on the pendulum model should be checked. This, however, is beyond the scope of present study.

As stated above, using constant height is an essential part in derivation of the pendulum-based response spectra. To utilize such spectra for derivation of the base-shear of MDOFs, the FSSDOF system is presented next.

4.3 Conceptual Representation of the FSSDOF System

For an SDOF system, limiting the SC is equivalent to setting an upper limit on the period of vibration (Bernal, 1992, 1998). This can be shown by rewriting Eq. (2.3) as:

$$T_0 = 2\pi\sqrt{\frac{\theta.h}{g}} \tag{4.2}$$

On the other hand, for MDOF systems, SC is defined at each storey separately. In analogy with SDOF systems, limiting SC at each level of a MDOF system is equivalent to imposing an upper limit on the "*Individual-Storey-Periods*". To show this, one notes that Eq.(2.3) can be rewritten as:

$$\theta_i = \frac{P_i}{K_{\Delta i}.h_i} = \frac{M_i.g}{K_{\Delta i}.h_i} \tag{4.3}$$

in which, M_i , is the total seismic mass above i^{th} storey, defined by (see Fig.3):

$$M_i = \sum_{j=i}^{N} m_j \tag{4.4}$$

where, m_j , represents the total seismic mass of the j^{th} storey and N represents the number of storeys. If i^{th} level is assumed as an inverted-pendulum with a height equal to its actual height, by use of Eq.(4.3), its period can be derived as:

$$T_i = 2\pi\sqrt{\frac{\theta_i.h_i}{g}} \tag{4.5}$$

which is same as Eq.(4.2), utilized to the i^{th} level. It follows that, for MDOF systems, limiting SC corresponds to limiting period of vibration of each storey,

modeled as an inverted-pendulum, with a weight equal to the total weight above it, and a height equal to its actual height. Such models are shown in Figure 4.3.

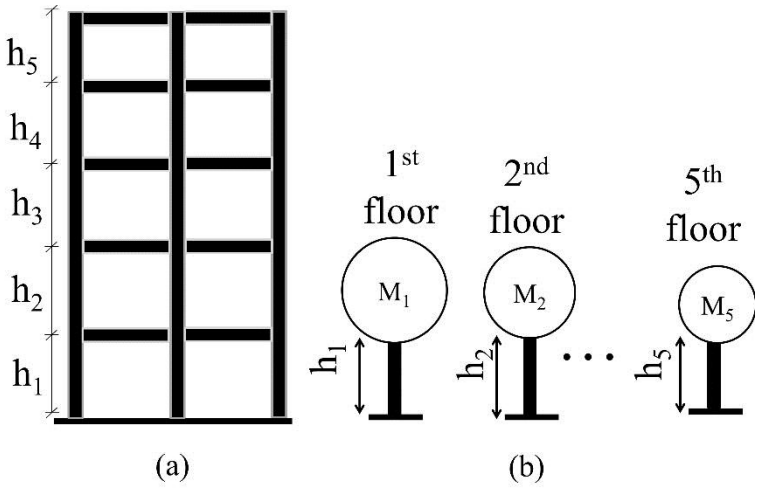

Figure 4.3: Conceptual presentation of Storey-wise SDOF systems. a) The original MDOF system, and b) Individual-Storey SDOF systems.

Compared to the fundamental period of vibration, with no restriction on it, individual-storey-periods present an effective tool. Particularly, limiting the individual-storey-periods enables the designers to estimate the necessary lateral stiffness of each storey. However, such a treatment demands for identifying the input motion at various levels, while it is usually known at the base of a structure. In addition, considering the interaction between floors is complicated. Having said this, among all levels of a MDOF, the first-storey is a special case since:

- Total axial load on the first-storey is equal to the total seismic load acting on the structure,
- the shear force at first-storey is equal to the base-shear,
- its height rarely changes during design, and,
- the input excitation at first-storey is known.

Owing to above listed properties, first-storey can be presented as a new SDOF system, namely: the FSSDOF system, with further practical advantages. It should be noted that, the FSSDOF is not aimed to present dynamic characteristics of the original MDOF system. It will solely be used as a practical tool that enables extension of the pendulum-based response spectra to MDOF systems.

Since the FSSDOF system is essentially a SDOF system with known height, it directly facilitates the implementation of the UPEM and SCRS for derivation of the base-shear and lateral seismic forces of MDOFs. Explicitly speaking, upon construction of a constant-ductility-response-spectrum exclusively utilized to the FSSDOF, the base-shear complying with a given ductility level can be found easily. Moreover, by limiting the initial period of the FSSDOF system, it is possible to satisfy code requirements regarding the SC at least at the first-storey.

For instance, Fig.4.1 can be considered to serve as the FSSDOF's response-spectra for a MDOF with a 3.0m long first-storey. As such, Eq. (4.3) can be used to find the minimum necessary lateral stiffness at the first-storey, compatible with a permissible SC. It follows that, by use of Eq. (4.5) and Fig.4.1, the base-shear complying with a given ductility level can be established.

It should be noted that the FSSDOF is not aimed to represent dynamic characteristics of the original MDOF system. It will solely be used as a practical tool that enables extension of the SCRS to calculate the necessary lateral stiffness of the first-storey of a MDOF.

On the other hand, since code specified limits are imposed on the SC and inter-storey drifts, it might be helpful if the FSSDOF spectrum is presented in a different format. To this end, the SCRS is presented in the next section.

4.4 The Stability Coefficient Response Spectra (SCRS)

Period-dependence feature of SC presents an outstanding opportunity for representing the pendulum based response spectra in terms of SC. For example, by use of Eq.(4.2), the constant ductility response spectra of Figure 4.1 are presented in the SCRS format, in Figure 4.4.

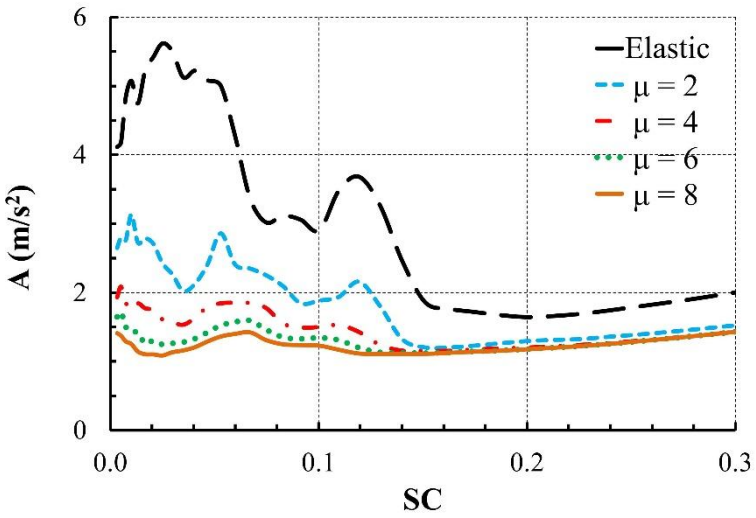

Figure 4.4: The response spectra of Figure (4.1) presented in the SCRS format.

Clearly, SCRS can be developed for any desired spectral parameter. For instance, Figure 4.5 represents the spectral displacement SCRS.

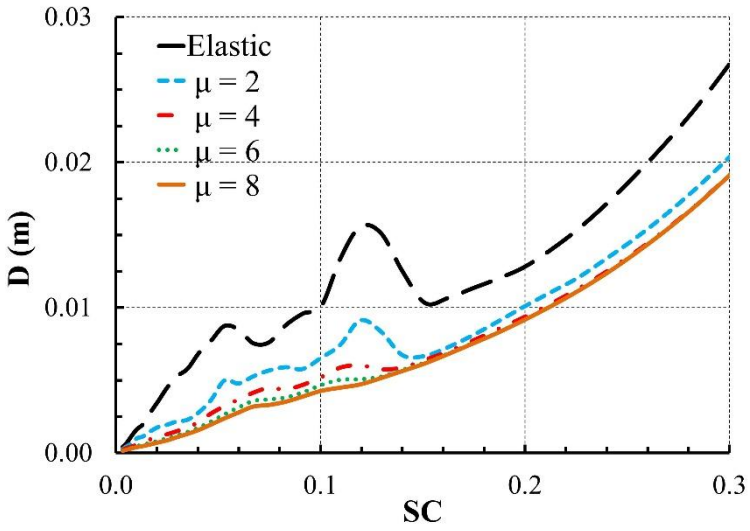

Figure 4.5: SC Response Spectra of Figure (5.1) plotted in terms of spectral displacement.

4.5 Verification Examples

It might be important to check reliability of the presented spectrum in estimating lateral forces acting on a structure in presence of P-delta effect. For this purpose, two numerical examples are presented in the following section. The first example is a SDOF and the second one is 5-storey Steel-Moment-Resisting-Frame (SMRF).

4.5.1 Example 1: SDOF System

Consider a one-storey, one-bay, reinforced concrete moment resisting frame. It is desired to derive the base-shear acting on the frame based on a conventional response spectrum and to compare the results to those calculated by use of the SCRS and FSSDOF system. The frame has a bay of 5.0 *m*, and a height of 3.0 *m*. Seismic weight acting on the frame consists of a 50 *kN/m* dead load and a 30 *kN/m* live load. It is assumed that the 1999 Kocaeli earthquake recorded at Yarimca sufficiently resembles the state of hazard.

Total seismic weight acting on the frame is W = 295 *kN*, in which 30% live load participation factor is considered. To use a conventional MSD spectrum, the

fundamental period of vibration, and hence, member sizes should be specified a priori. Initially, a square cross-section (30 *cm*) is selected for all members. Modal analysis revealed an initial period of vibration of T_1=0.35(*s*) for this frame. The base shear coefficients, lateral displacements, and corresponding SCs for four levels of ductility are summarized in Table 4.2.

Table 4.2: Base-shear, lateral displacement and SC based on conventional MSD model (example 1).

μ	2	4	6	8
Base-shear-Coefficient =A/g	0.317	0.177	0.140	0.120
Base-Shear, V_1 (kN)	93.52	52.22	41.30	35.40
Lateral Displacement, Δ (m)	0.0087	0.0049	0.0038	0.0032
θ	0.0091	0.0092	0.0090	0.0089

As explained earlier, by use of the SCRS, establishing the member sizes is not necessary; instead, one can select a desired SC for the first-storey and consult with the spectra of Figure 4.4. For example, if θ = 0.0092 is selected, the base-shear coefficient complying with $\mu = 2$ is read as: $A = 0.322\ g$. This will result in a base-shear of V = 95 *kN*. Now, by applying a lateral force of 95 *kN* on the frame, the maximum lateral displacement is calculated as: $\Delta = 0.0087\ m$. Results of such analysis repeated for other levels of ductility are summarized in Table 4.3.

Table 4.3: Base-shear, lateral displacement and SC based on SCRS (example 1).

μ	2	4	6	8
Base-Shear-Coefficient = A/g	0.322	0.18	0.15	0.13
Base-shear, V_1 (kN)	95	53.1	44.25	38.35
Lateral Displacement, Δ (m)	0.0087	0.0049	0.004	0.0035
θ	0.0092	0.0092	0.0089	0.0090

It can be seen that the SCRS gives slightly higher results (compare Tables 4.2 and 4.3), which is due to inclusion of the P-delta effect. However, and in agreement with

current state-of-practice, P-delta effect is quite negligible for small values of SC. More importantly, using the SCRS makes derivation of the base-shear of a SDOF system a one-step procedure; in other words, calculating the initial period of vibration, and hence, preliminary selection of the member sizes, is not necessary. Specifically, by use of Eq.(4.2), and setting the SC to a suitably selected value, the base-shear complying with a desired level of ductility can be found directly.

4.5.2 Example 2: MDOF System

As discussed earlier, Asimakopoulos et al. (2007) proposed a method for inclusion of the P-delta effect into the DDBD procedure. The method assumes that the maximum value of the dynamic-SC (the SC calculated under dynamic loading) over the height of a MDOF system sufficiently resembles the SC of the corresponding ESDOF system. Applicability of their method was shown on a numerical example, which is adopted here.

Consider a two-bay, five-storey, steel-moment-resisting-frame with storey heights and bay widths equal to 3.0, and 4.0 *m*, respectively. The seismic weight acting on the structure is calculated based on a dead load of 25 *kN/m*, the self-weight of the frame members, and a live load of 10 *kN/m*. Live load participation factor is set to 30%. Initially, IPE-300 and HEB-260 are used for beams and columns, respectively. The fundamental period of vibration was calculated as T_1 = 1.242 (*s*). Here again, it is assumed that the 1999 Kocaeli earthquake, recorded at Yarimca, fully specifies the state of hazard.

First, and based on a conventional response spectrum without P-delta effect, the base-shear and lateral forces are calculated. For T_1 = 1.242(s) the base-shear coefficient is equal to 0.185*g*. This results in a base-shear of: $0.185 \times 1201.778 =$

$222.32\ kN$. After calculating the storey-wise lateral drifts and corresponding SCs, the floor shears are increased by the amplification factor $\alpha_i = 1/(1-\theta_i)$ defined in Eurocode 8. For the new set of lateral forces, the lateral drifts and corresponding SCs are re-calculated. Next, by use of the SCRS and FSSDOF system, and by setting the SC to the one which is calculated at the first-storey, a new base-shear is calculated. Results are summarized in Tables 4.4 and 4.5. In addition, the difference in calculated drifts, floor forces, and floor shears are depicted in Figure 4.6.

Results indicate that the FSSDOF system is quite capable of estimating storey-wise forces. The maximum difference between the FSSDOF and original case (without P-delta effect) in estimating the floor shears reaches to 15.57%, which is due to inclusion of the P-delta effect. When compared to the amplified seismic actions, the FSSDOF estimates are higher, and vary between 10.18 to 13.91% at various floors.

Table 4.4: Results of example 2.

	Mass-Spring (Without P-delta)			Amplified		
Floor	Lateral Force (kN)	Drift (m)	SC	Lateral Force (kN)	Drift (m)	SC
1	15.15	0.0208	0.0376	15.75	0.0217	0.0377
2	29.78	0.0299	0.0461	31.23	0.0312	0.0459
3	44.68	0.0272	0.0367	46.38	0.0282	0.0367
4	59.57	0.0208	0.0250	61.09	0.0215	0.0252
5	73.14	0.0125	0.0135	74.17	0.0127	0.0135

Table 4.5: Results of example 2 (continued).

	Mass-Spring (Without P-delta)			FSSDOF (SCRS)		
Floor	Lateral Force (kN)	Drift (m)	SC	Lateral Force (kN)	Drift (m)	SC
1	15.15	0.0208	0.0376	17.51	0.0241	0.0376
2	29.78	0.0299	0.0461	34.41	0.0347	0.0463
3	44.68	0.0272	0.0367	51.61	0.0316	0.0369
4	59.57	0.0208	0.0250	68.82	0.0241	0.0250
5	73.14	0.0125	0.0135	84.50	0.0148	0.0138

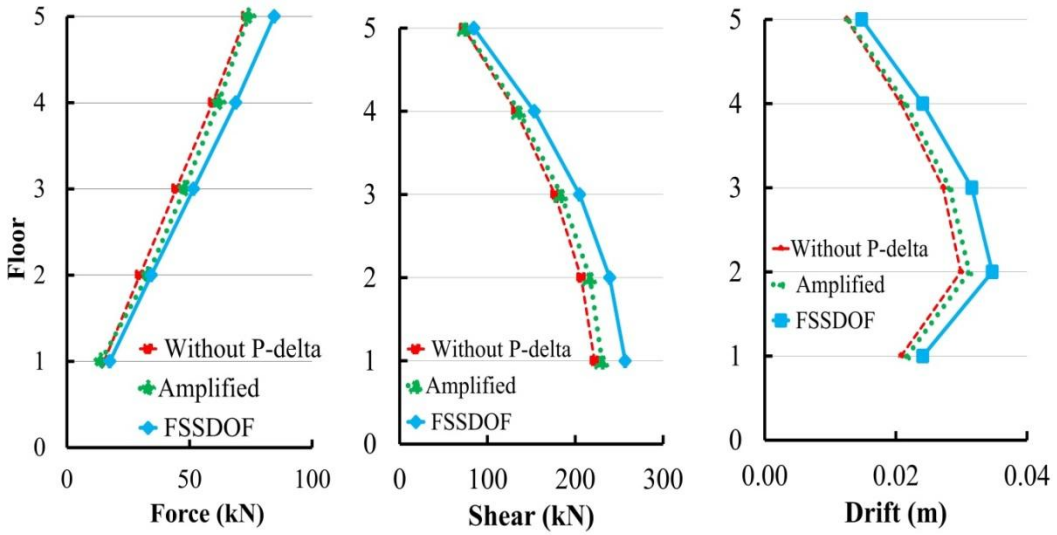

Figure 4.6: Example 2: a) Lateral force distribution, b) Shear distribution, and c) Drift distribution.

Using DDBD and based on extensive time history analysis, Asimakopoulos et al. (2007) reported a 10.9% increase in the floor shears, compared to the case without P-delta, which well agrees with the presented results. In the mentioned study, a smooth code-based design spectrum was used. However, in the above example a very jagged single record response spectrum is used, and hence, observing small deviations is not surprising. Additionally, underestimation of the Eurocode 8 amplification factors was reported in their study.

The advantage of the FSSDOF system over the conventional MSD model is in the fact that by use of Eq.(4.5) and Figure 4.4, one can proceed with selection of the first-storey member sizes that comply with a given SC and code specified limits. Having said this, the maximum SC does not necessarily occur at the first-storey. For example, Tables 4.4 and 4.5 show that the maximum SC is calculated at the second-storey. This is not important in the above presented example since the calculated SCs are well below code specified limits. Nonetheless, satisfying the SC limits at the

first-storey will present the minimum necessary lateral stiffness, and hence, minimum required member sizes at the first-storey.

A further comparison of the results is performed against the relation proposed by Asimakopoulos et al. (2007) for the maximum storey-wise SC under dynamic loading. The mentioned relation estimates the maximum SC under dynamic loading as a function of the number of stories *n* and the ratio of the moment of inertia of the cross-section of columns to those of beams n_1. For the above presented example, with $1.5 < n_1 < 2.0$, one has:

$$SC = \alpha n^b = 0.015 \times 5^{0.76} = 0.05 \quad (4.6)$$

where values of α and b correspond to subsoil class C. The FSSDOF system gives the maximum SC equal to 0.0463 at the second storey, which well agrees with 0.05.

Noticeably, derivation of the base-shear and storey-wise lateral forces based on the SCRS and FSSDOF is period independent. In other words, setting preliminary dimensions for the members is not necessary; rather, selection of member sizes at the very early stages of a design process can be enhanced.

4.6 FSSDOF System in the Context of Yield-Point-Spectra Method

4.6.1 Pendulum Model Versus Mass-Spring System in Derivation of YPS

Although limiting the SC is an important step in seismic resistance design, controlling the drifts usually imposes a more restrict condition on the final design. To control drifts, just like the SC, a designer should derive the floor forces and analyses the structure several times, with each step requiring the calculation of a new set of lateral forces (owing to changes in fundamental period). Obviously, this will result in more trials.

In their study, Aschheim and Black (2000), showed that the YPS, which is a constant-ductility-response-spectrum in terms of the yield-displacement versus spectral acceleration, can greatly enhance controlling displacements in a DDBD context. They advanced the method to include the P-delta effect through introducing the "effective-height" concept in a later study (Aschheim & Montes, 2003). The effective height was defined as the product of actual height by the ratio of the dead load to the total vertical load (dead plus live load). Having said this, the method does not recognize the period-dependent feature of SC. Explicitly speaking, P-delta effect is introduced by linearly increasing the spectral acceleration of a MSD model by a factor, which is inversely proportional to the effective-height (Aschheim & Montes, 2003). Consequently, and by increasing period, a systematic underestimation of the P-delta effect can be observed in this method as well. Nevertheless, the idea behind the YPS method, which is plotting spectral acceleration versus yield-displacement, presents great opportunities for further improvements.

If the constant-ductility-response-spectra of the pendulum model are plotted in terms of the yield-displacement, a modified version of the YPS in which period-dependence of SC is considered will result. For example, Figure. 4.7 shows the difference between pendulum model (modified) and MDS model (original) in derivation of the YPS. The P-delta effect is included in both modified and original YPS. Also, note that the modified YPS of Figure 4.7 is essentially a different presentation of Figure 4.1. On the other hand, establishing the effective-height is necessary for plotting the original YPS. An effective-height equal to the pendulum's height (3.0 m) is adopted for construction of Figure 4.7. Additionally, the spectra of Figure 4.7 are constructed up to the same initial period, not the same yield-displacement. Moreover, to emphasize on permissible SC values, results are limited

to a pendulum's period of 2.0 (s), which results in a maximum first-storey yield-displacement of $0.015m$. Other assumptions are same as those assumed for construction of Figure 4.1.

It can be seen that the divergence between the conventional and modified YPS is more significant for highly ductile systems. Effect of various levels of ductility on the modified YPS is depicted in Figure 4.8.

The modified YPS accounts for the period-dependent feature of SC. Therefore, its application can be extended to MDOFs through the FSSDOF system. This will allow accounting for the displacement limits at the early stages of a design project; and hence, will present a yet more practical starting point. The mentioned issue is shown on a numerical example in the next subsection.

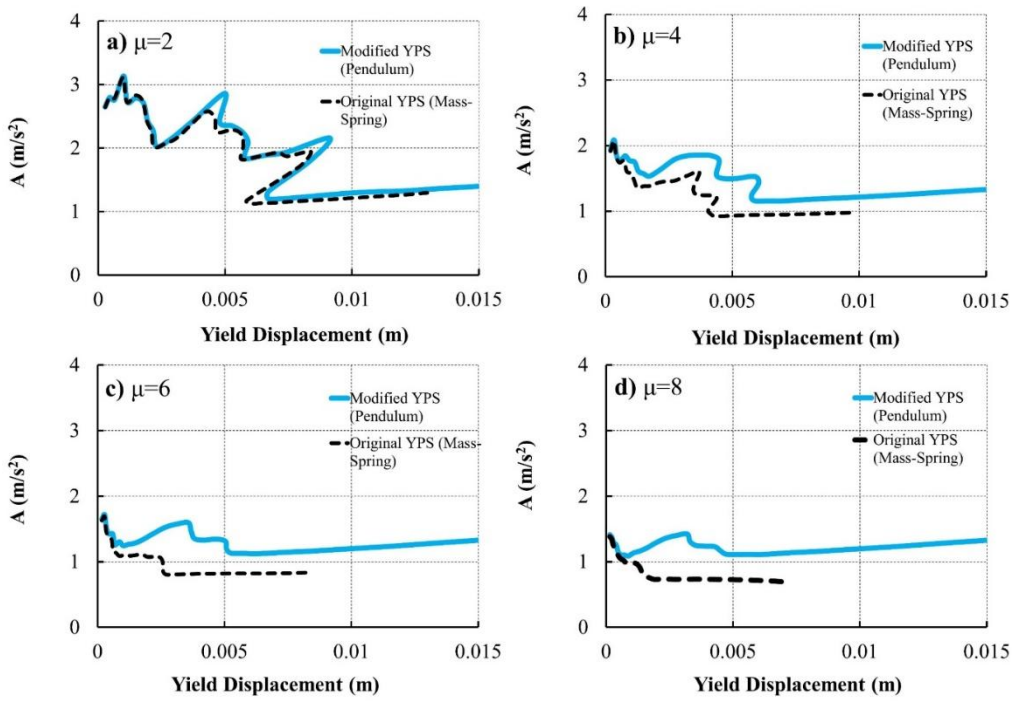

Figure 4.7: Comparing original YPS derived base on mass-spring and pendulum models for various levels of ductility; a) μ=2, b) μ=4, c) μ=6, and, d) μ=8.

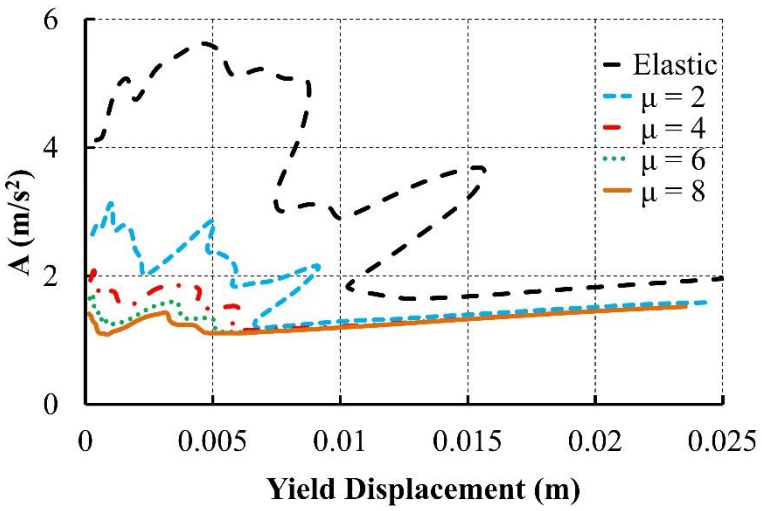

Figure 4.8: Yield point spectra based on pendulum model for various levels of ductility (μ=2,4,6 and 8).

4.6.2 Example 3

EC8 specifications, demand for inter-storey drifts to be limited, under a seismic action having a larger probability than the design seismic action corresponding to no-collapse requirements. The limitations depend on brittleness of the non-structural elements. On the other hand Turkish seismic design specifications (TEC, 2018), demand for inter-storey drifts to be limited to $0.0035h_i$ in all conditions. In this example, the latter requirement will be followed.

Suppose that for the given five-storey frame of example 2, it is desired to find member sizes to satisfy drift limitations imposed by Turkish standards. Obviously, this can be achieved by increasing lateral stiffness of the frame through several trials. However, as the lateral stiffness changes (increases) fundamental period of vibration also changes (decreases) and hence in each step a new set of lateral forces should be calculated. For the analysis, again it will be assumed that Kocaeli *at* Yarimca record fully defines the state of hazard. Table 4.6 summarizes some accomplished trials to

satisfy inter-storey drifts. Note that some intermediate trials are not presented for the sack of brevity.

Table 4.6: Some selected iterations performed for example 3 to satisfy drift ratio limits.

Floor	**1st trial IPE300 HEB300 (T_1= 0.93s)**		**2nd trial IPE330 HEB320 (T_1= 0.90s)**		**3rd trial IPE330 HEB340 (T_1=0.85s)**		**4th trial IPE400 HEB400 (T_1=0.67s)**	
	Force	$(\Delta_i)/h$	**Force**	$(\Delta_i)/h$	**Forces**	$(\Delta_i)/h$	**Forces**	$(\Delta_i)/h$
1	18.92	0.0070	18.68	0.0037	20.48	0.0037	16.38	0.0018
2	37.19	0.0113	36.71	0.0061	40.25	0.0061	32.20	0.0029
3	55.79	0.0107	55.06	0.0059	60.37	0.0059	48.30	0.0028
4	74.38	0.0082	73.41	0.0046	80.50	0.0046	64.40	0.0022
5	91.33	0.0050	90.14	0.0030	98.84	0.0030	79.07	0.0014

Based on above trials a more refined result, with T_1=0.7s, and a base-shear of 252.37kN, was obtained. Frame members, floor forces, and corresponding drift ratios are presented in Table 4.7.

Table 4.7: Finalized member sizes and corresponding drift ratios at various levels for example 3.

Floor	Beams	Columns	Forces (without P-delta)	$(\Delta_i)/h$
1	IPE-400	HEB-400	17.20	0.0019
2	IPE-400	HEB-400	33.81	0.0032
3	IPE-360	HEB-360	50.71	0.0035
4	IPE-360	HEB-360	67.62	0.0030
5	IPE-360	HEB-360	83.03	0.0020

If it was known from the beginning that the drift ratio at the first-storey is to be limited to 0.0019, by consulting with the spectra of Figure 4.8, one would have been able to calculate the final result in one-step. For the given frame, if drift ratio at the first-storey is limited to 0.0019, the spectrum of Figure 4.8 gives a base-shear coefficient of 0.225g, with a corresponding base-shear of 270.4 kN. Compared to the previously calculated base-shear, this means a 6% difference, which is because of P-delta effects.

The calculated base-shear is then used to derive a new set of lateral forces and the resultant storey-wise drift ratios, together with those calculated through time history analysis are presented in Table 7. It can be seen that the differences are quite negligible.

Table 4.8: Comparing drift ratios calculated based on the modified YPS to the time history results (example 3).

Floor	$(\Delta_i)/\boldsymbol{h}$	
	Modified YPS by use of the FSSDOF	Time History
1	0.0020	0.0016
2	0.0033	0.0027
3	0.0037	0.0030
4	0.0032	0.0026
5	0.0021	0.0017

Having said this, one needs a prior knowledge on the drift ratio limit at the first-storey such that code requirements at all other levels are satisfied. In absence of such information, it is possible to set the minimum necessary lateral stiffness, based on drift ratio limits at the first-storey.

Chapter 5

EFFECT OF VERTICAL COMPONENT OF GROUND MOTION ON GLOBAL RESPONSE

5.1 Introduction

As stated earlier, evaluating the potential effects of the VCGM on the global response has been the subject of some studies. Effect of the VCGM could be considered in two categories. First, it may initiate some modes of failure, like over-compression, and second, it could adversely influence the horizontal response through altering the P-delta effect. The latter is a result of variations of the gravitational acceleration, and hence seismic weight, upon action of the VCGM.

On the other hand, previous literature indicates on the unfavorable effect of the P-delta effect on the maximum-inelastic-horizontal-response (C Adam & Ibarra, 2015; Christoph Adam & Jäger, 2012a; Amara et al., 2014; Asimakopoulos et al., 2007; Bernal, 1998; Gupta & Krawinkler, 2000; Jough & Şensoy, 2016; López et al., 2015; Rahimi & Estekanchi, 2015). Henceforth, it seems quite reasonable to expect variations of the horizontal response upon inclusion of the VCGM in the analysis.

However, potential influences of the VCGM on the maximum-inelastic-horizontal-response, and specifically, its capability to initiate dynamic instability is still a matter of question. This might be due to the fact that during field observation representing confident evidence for damage from VCGM is a challenging task (Kunnath, Erduran,

Chai, & Yashinsky, 2008). Accordingly, distinguishing possible effects of the VCGM on the horizontal response might be even more challenging. Hence, theoretical approaches might be necessary.

In response to above mentioned issues, present study discusses: (i) the significance of inclusion of the VCGM on the P-delta effect, and in turn, on the maximum-inelastic-horizontal-response of SDOFs, especially at far distances from the source, (ii) the influence of the initial period of vibration and strength reduction factor on deviations of the horizontal-response of SDOFs upon inclusion of the VCGM, and particularly, (iii) capability of the VCGM to initiate dynamic instability.

5.2 Record Selection and Framework

Among various parameters, which may have influential impacts on the response under coupled action of earthquake components, present study tries to highlight effects of period of vibration and strength reduction factor. To this end, and by means of time-history analysis, the maximum-inelastic-horizontal-response under biaxial excitation, $\emptyset^{H+V}$, is compared to the corresponding response under uniaxial excitation, $\emptyset^{H}$.

The main reason for selecting the maximum-inelastic-response as the representative engineering parameter is that comparing maximum response of various systems, with different characteristics, is a well-tested routine in earthquake engineering (Ruiz-García & Miranda, 2003). In addition, maximum response has found various applications, like calculation of the ductility-demand imposed on a system (Chopra, 2007), quantification of the state of damage (Williamson, 2003), evaluation of

collapse through monitoring the maximum response under incrementally increased excitations (Vamvatsikos & Cornell, 2002), etc.

To evaluate effects of the VCGM present study uses time-history-analysis. Having said this, application of time-history analysis demands for careful selection of input motions (C. Haselton et al., 2012). Obviously for the purpose of present study the record selection scheme cannot be based on currently available selection and scaling strategies. This is mainly due to the fact that the available record selection methods use uncoupled mass-spring vibrators in horizontal and vertical directions (Baker & Lee, 2017). Hence, although a given set of recorded motions may appropriately represent the state of hazard in one direction, its effectiveness in representing the state of hazard under coupled action of earthquake components is not clear (Çağnan et al., 2017). Therefore, one may need to separately select vertical and horizontal components, which might logically be questioned.

Therefore, present study follows two steps to avoid undesirable bias. The first step, which focuses on examining the influence of some important parameters, and evaluating possible effects of the VCGM at far field, adopts a set of 12 records based on an event based record selection scheme. In other words, specific examples from available recorded motions corresponding to three major events, Table 5.1, are carefully selected to enhance further discussions. The second step evaluates capability of the VCGM to initiate dynamic instability. This step adopts a set of 26 records, Table 5.2, which resembles an assumed target spectrum, Figure 5.1, at a near field site. Moreover, previous literature indicates that the SC (Eq.(2.6)) is a period-dependent parameter and reliable treatment of the P-delta effect demands for

consideration of this issue (Aydınoğlu & Fahjan, 2003). Therefore, in this study period-dependence of the SC is considered.

Table 5.1: 12 records corresponding to three major events of 1994 Northridge (USA), 1995 Kobe (Japan), and 1999 Kocaeli (Turkey) earthquakes.

Event	Magnitude	station	R_{jb} (km)	PGA_H (g)	V/H	V_{s30}(m/s)
Kocaeli	7.51	Yarimca	1.38	0.23	0.92	297
		Iznik	30.73	0.12	0.60	476
		Istanbul	49.66	0.04	0.69	595
		Duzce	13.6	0.31	0.65	281
Northridge	6.69	Arleta Nord Hoff Fire Sta.	3.30	0.34	1.6	297
		La Saturn	21.17	0.47	0.21	308
		Antelope Butts	46.65	0.10	0.42	572
		Newhall W-Pico Canyon	2.11	0.42	0.70	285
Kobe	6.90	Kobe University	0.9	0.27	1.66	1043
		Kakogawa	22.5	0.24	0.71	312
		Chihaya	49.91	0.11	0.64	609
		Port Island	3.31	0.29	1.97	198

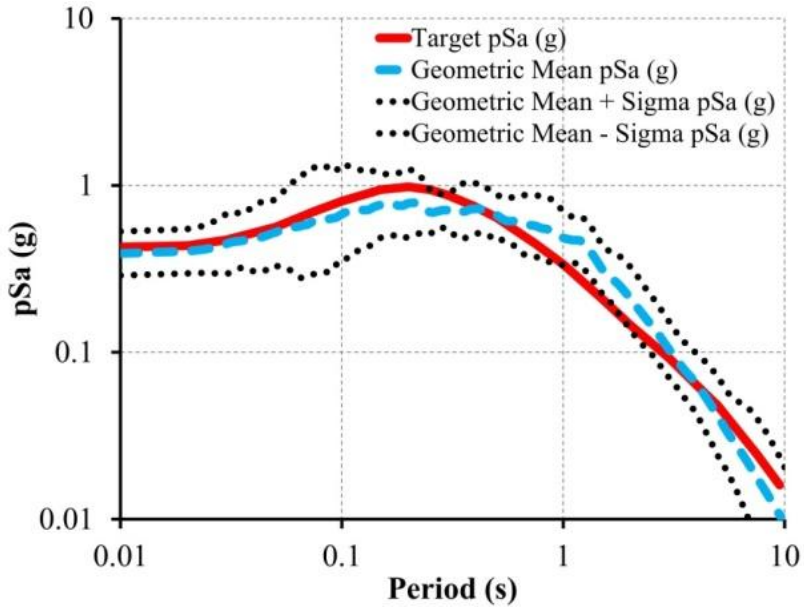

Figure 5.1: The selected target spectrum for the second step of analysis.

Table 5.2: The set of selected records complying with the target spectrum of Figure 11.

Earthquake	Year	Station	Magnitude	R_{jb} (km)	R_{rup} (km)	Component	PGA_H (g)	V/H
Imperial Valley-06	1979	Agrarias	6.53	0.00	0.65	AGR003	0.28	1.64
						AGR273	0.19	2.47
Imperial Valley-06	1979	El Centro Array #5	6.53	1.76	3.95	E05140	0.53	1.11
						E05230	0.38	1.55
Superstition Hills-02*	1987	Parachute Test Site	6.54	0.95	0.95	B-PTS225	-	-
						B-PTS315	-	-
Landers	1992	Lucerne	7.28	2.19	2.19	LCN260	0.72	1.14
						LCN345	0.79	1.04
Kobe-Japan	1995	KJMA	6.90	0.94	0.96	KJM000	0.83	0.40
						KJM090	0.62	0.53
Kobe-Japan	1995	Takarazuka	6.90	0.00	0.27	TAZ000	0.69	0.61
						TAZ090	0.61	0.69
Kobe-Japan	1995	Takatori	6.90	1.46	1.47	TAK000	0.67	0.42
						TAK090	0.61	0.46
Bam-Iran	2003	Bam	6.60	0.05	1.70	BAM-L	0.80	1.21
						BAM-T	0.63	1.54
Parkfield-02-CA	2004	Parkfield - EADES	6.00	1.37	2.85	EADES-90	0.32	0.59
						EADES360	0.39	0.49
Parkfield-02-CA	2004	Parkfield - Cholame 1E	6.00	1.66	3.00	C01090	0.44	0.52
						C01360	0.36	0.64
Parkfield-02-CA	2004	Parkfield - Fault Zone 9	6.00	1.22	2.85	Z09090	0.15	0.63
						Z09360	0.097	0.97
Darfield-New Zealand	2010	GDLC	7.00	1.22	1.22	GDLCN5W	0.76	1.63
						GDLCS35W	0.70	1.77
Duzce-Turkey	1999	IRIGM 487	7.14	2.65	2.65	487-NS	0.3	0.76
						487-EW	0.28	0.82

** indicates that vertical component of the mentioned record was not available and hence it was eliminated from the analysis.*

5.3 Variation of Stability Coefficient

Close inspection of Eq.(2.1) shows that the P-delta effect and VCGM similarly affect a system's resistance. However, they may magnify or reduce each other's effect depending on whether VCGM acts in-phase with the gravitational acceleration or not (Graizer & Kalkan, 2008). This might be shown by noting that upon action of the VCGM, and in analogy with Eq.(2.3), Eq.(2.6) can be modified as:

$$\mathrm{SC_V} = \theta_V = \frac{P + P^*}{K_{\emptyset 0.}} h = \frac{\omega_{GV}^2}{\omega_0^2} \tag{5.1}$$

where, $SC_V = \theta_V$ denotes the SC in presense of theVCGM, $P^* = m\ddot{x}_v$, and, $\omega_{GV}^2 = (g + \ddot{x}_v)/h$. It follows that, Eq.(2.7) might be modified as:

$$mh^2\ddot{\emptyset} - \omega_{GV}^2 \sin\emptyset + m\ddot{x}_h h\cos\emptyset + M(\emptyset) + c_\emptyset\dot{\emptyset} = 0 \tag{5.2}$$

In addition, owing to time-dependent variations of $\ddot{x}_v$, $\mathrm{SC_V}$ is a dynamic variable. For example, Figure 5.2 shows time-dependent variations of the SC under action of the vertical component of 1995 Kobe earthquake, recorded at Port Island.

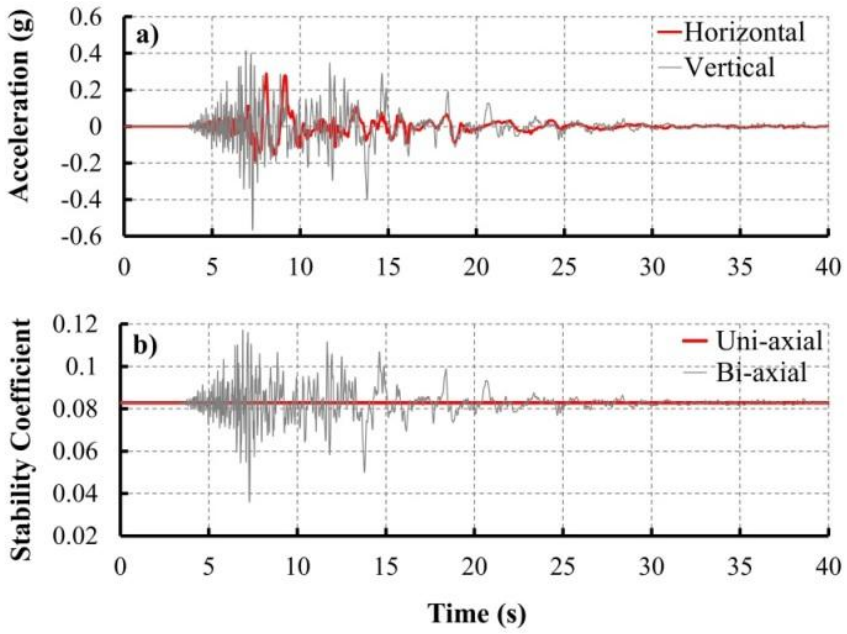

Figure 5.2: a) horizontal and vertical acceleration time histories of the1995 Kobe earthquake recorded at Port Island, b) time-dependent variations of the SC under uniaxial (constant) and bi-axial excitations of the same record.

This phenomenon indicates that in a given time instance the value of SC_V might be significantly different from SC. Therefore, VCGM may significantly affect the maximum-inelastic-horizontal-response, and in turn, the state of damage (Williamson, 2003).

Moreover, although coincidence of vertical and horizontal peaks might be considered as the worst scenario, happenstance of a sufficiently large vertical acceleration with a sufficiently large horizontal one is enough to considerably alter a system's SC, and consequently, its inelastic response. Thus, value of the vertical acceleration in a decisive time instant, and whether it acts in-phase with gravitational acceleration or not, may significantly affect a system's performance.

5.4 Analysis and Results

As mentioned above, this study is accomplished in two steps. In the first step, and by use of the set of recorded motions of Table 5.1, maximum-inelastic-rotations of 5% damped bilinear SDOF systems, with a post-yield stiffness equal to 5% of the initial stiffness, under bi-axial excitations are compared to their uniaxial counterparts. Systems with initial periods between 0.2 to 2.0s, with four levels of strength reduction factor (R=2,4,6 and 8) are considered. Detailed time history analysis reveals that both period of vibration and strength reduction factor influence the maximum-inelastic-horizontal-response under biaxial excitation. Figure 5.3 demonstrates the average fluctuations of the maximum-inelastic-rotations due to action of the VCGM over the selected records.

On average, effet of the VCGM on maximum-inelastic-horizontal-response is significant for systems with initial periods ranging from 1.0 to 2.0s. This might be

attributed to the period-dependent feature of SC. In the short period range, value of the SC is so small that it does not affect the response, even though presence of the VCGM fluctuates it. On the other hand, for long period systems, and even under uniaxial excitation, the SC becomes so large that results in negative-post-yield-stiffness, which in turn causes dynamic instability. Henceforth, effect of VCGM may be considered as to increase the rate with which dynamic instability occures.

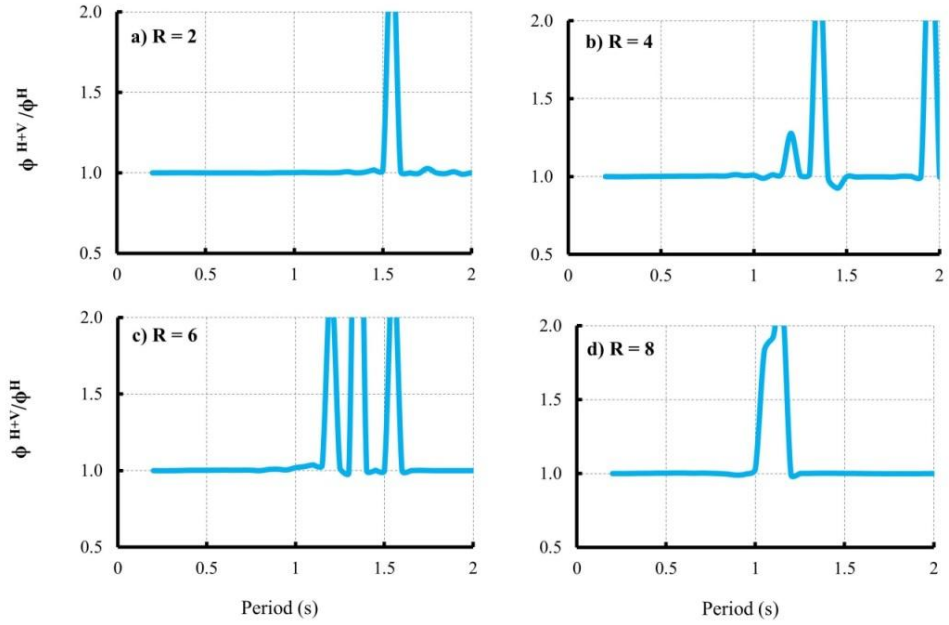

Figure 5.3: Ratio of maximum inelastic rotation under biaxial excitation, MIR_{V+H}, to the maximum inelastic rotation under horizontal excitation only, MIR_{H}. (R=2, 4, 6 and 8).

In contrast, effect of VCGM is quite significant for,say, medium range of initial periods. In the mentioned range, SC is large enough to approximately cancel the hardening. As a result, for some records, and upon inclusion of VCGM, system may experince negative-post-yield-stiffness while its counterpart under uniaxial excitation still shows positive or zero post-yield-stiffness. Therefore, difference between responces under bi-axial and uniaxial excitations are more significant in the medium range of initial periods.

Because of strong record-to-record variation of results, and following the event-based selection of records, in the subsequent section an event-based discussion is presented.

5.5 Event-Based Discussion of Results

5.5.1 Event 1: Kocaeli Earthquake

On the 17 August 1999 an earthquake occurred on the North-Anatolian-Fault with devastating consequences. The Kocaeli earthquake was a magnitude 7.51 strikeslip earthquake, which struk the densly occupied residential and industerial regions in the Turkey. The event caused serious casualties as well as great economic losses (Erdik, 2001). The event was recorded at various stations and substantially added to existing near field data. The Kocaeli earthquake has been followed by extensive studies and has gained some international importance for further research (Bommer et al., 2002; Erdik & Nuray Aydinoglu, 2011). Having said this, possible effects of VCGM on the horizontal response, and consequently, on the degree of experienced damage during the Kocaeli earthquake has received lesser attention.

As showm in Table 5.1, four of the recorded motions corresponding to Kocaeli earthquake were used in this study. Figure 5.4 shows the ratio of the maximum-inelastic response under biaxial excitation to the uniaxial one for the mentioned records. It can be seen that VCGM increases the horizontal respose at Yarimca and Iznik, decreases the response at Duzce, and has trivial effect on the response at Istanbul.

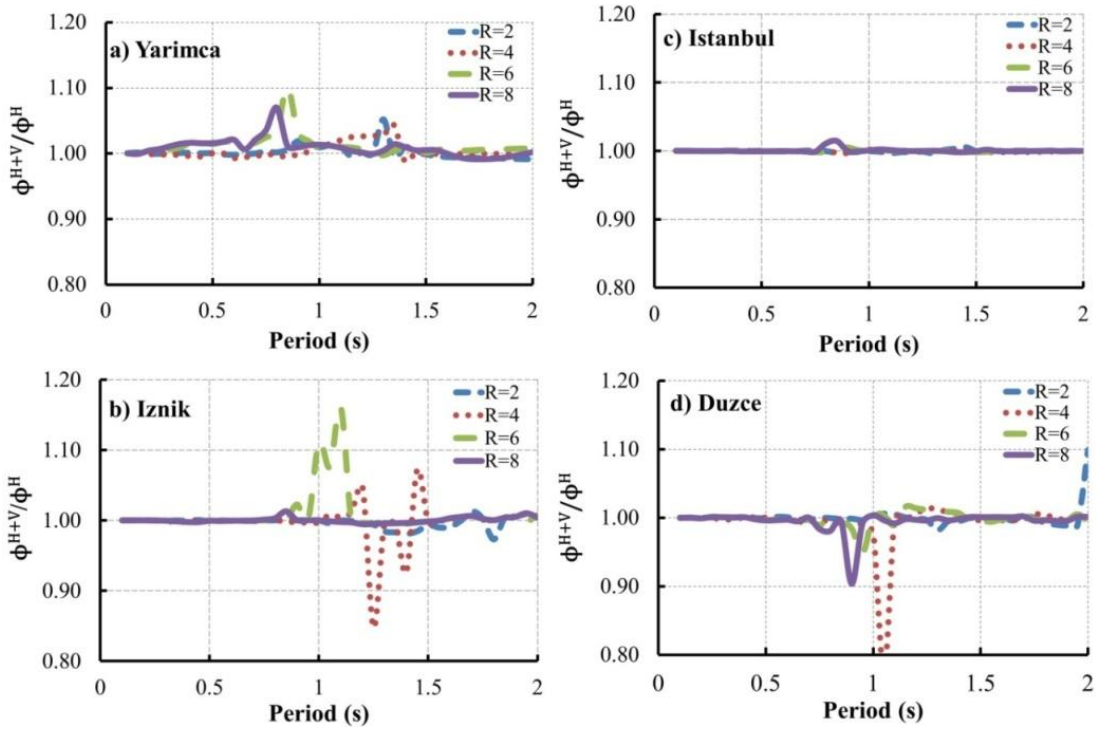

Figure 5.4: Ratio of the maximum-inelastic horizontal response under biaxial excitation to the maximum-inelastic horizontal response under uniaxial excitation under action of 1999 Kocaeli earthquake recorded at: a) Yarimca, b) Iznik, c) Istanbul and d) Duzce.

While effect of the period of vibration can be explained based on period-dependence of SC, effects of strength reduction factor and distance to source present great complications. Explicitly, while in previous literature effect of VCGM is considered to be more significant at near fault regions, Figure 5 shows that its maximum effect on horizontal response corresponds to Iznik record, some 30 km away from the source. This might be attributed to the fact that in evaluating possible effects of VCGM, previous studies are mostly focused on its engineering characteristics (Elgamal & He, 2004), not its effect on horizontal response.

On the other hand, for the two records which inclusion of the VCGM resulted in increased inelastic response (Yarimca and Iznik), situation is more serious for highly ductile systems (R=6 and 8). Even at Istanbul, where VCGM has almost no effect on

the response, very little variations of the response can be observed for R=8. Contradictory, under action of Duzce record, response of highly ductile systems is reduced. Furthermore, under action of Iznik record, and for a system with R=4, upon inclusion of VCGM, both increase and decrease of the horizontal response can be observed.

5.5.2 Event 2: Kobe Earthquake

The January 17, 1995 Kobe earthquake was a magnitude 6.9 strike slip earthquake which was considered one of the most sever events in the past century (Horwich, 2000). The event is another example which clearly demonstrates destructive potential of VCGM (Papazoglou & Elnashai, 1996). Variation of the ratio of the maxumum-inelastic horizontal response under bi-axial excitation, to the uniaxial one, under action of four records (Table 5.1) correspnding to Kobe earthquake are shown in Figure 5.5. This example not only confirms the previously presented difficulties regarding interpreting effects of distance to source and R-factor, but also provides evidence for capability of VCGM to initiate dynamic instability.

Figures 5.5-a, b and c show that variation of the maximum-inelastic response, with the exception of Chihaya record for R=2, remains within $\pm$ 5%. For the Chihaya record, however, maximum response of a system with R=2 shows an increase of about 15%. Considering the distance of the recording station, Chihaya record is another example which violates the general idea of negligible effect of VCGM at far distances. On the other hand, the Kobe university and Kakogawa records show a clear contradiction regarding influence of strength-reduction factor. Under action of Kobe university record, inclusion of VCGM increases the response of highly ductile and ductile systems. Contradictory, for Kakogawa record, VCGM causes a reduction

in the response of highly ductile systems while it increases the response of systems with low levels of ductility.

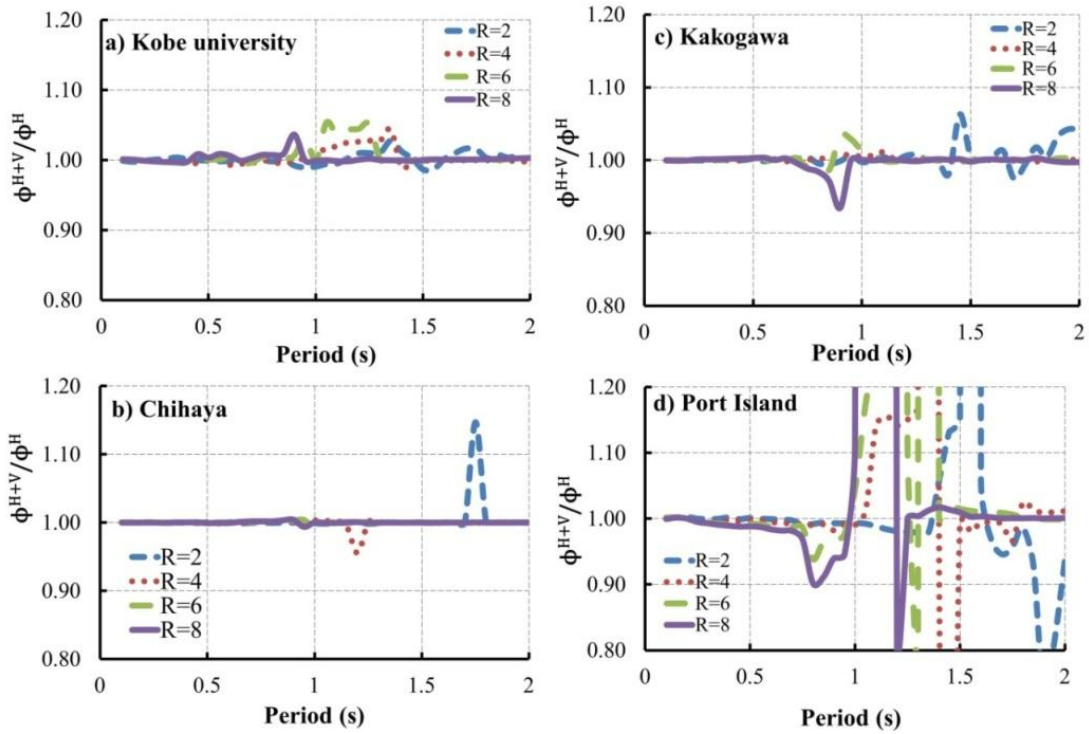

Figure 5.5: Ratio of the maximum-inelastic horizontal response under biaxial excitation to the maximum-inelastic horizontal response under uniaxial excitation under action of 1995 Kobe earthquake recorded at: a) Kobe University, b) Chihaya, c) Kakogawa and d) Port Island.

The Port Island record obviously shows the most interesting results. Boundary of the Figure 6-d is limited to 1.2 for presentation consistency. However, the results show significantly larger values, which might be considered as an indication for collapse. Due to attention-grabbing results of the Port Island record, full range of the Figure 5.5-d is replotted in Figure 5.6.

Figure 5.6 can be considered as a clear example which indicates capability of VCGM to cause collapse. Under action of the mentioned record, and for all levels of the strength reduction factor, the inelastic response under biaxial excitation is

substantially larger than its counterpart under uniaxial excitation. The amount of difference identifies that the system under bi-axial excitation might have collapsed. This is confirmed in Figure 5.7, where evolution of inelastic-response for a system with an initial period of T = 1.35s and R=6, under uniaxial and biaxial action of the Port Island record, are compared.

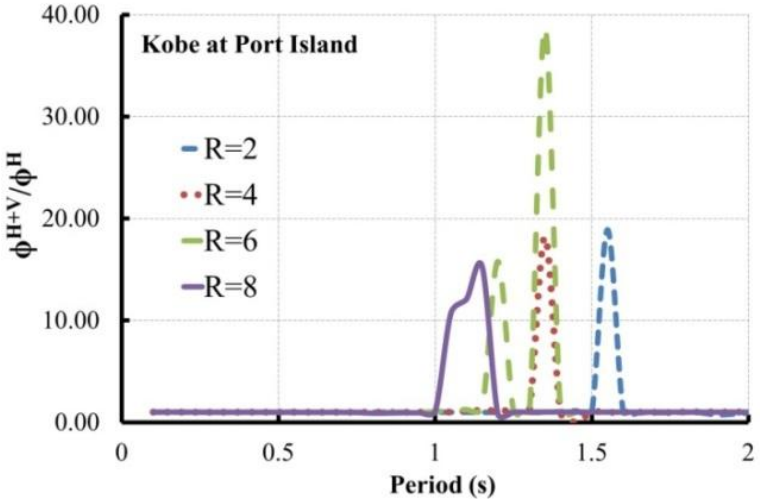

Figure 5.6: Ratio of the maximum-inelastic horizontal response under biaxial excitation to the maximum-inelastic horizontal response under uniaxial excitation under action of 1995 Kobe earthquake recorded at Port Island.

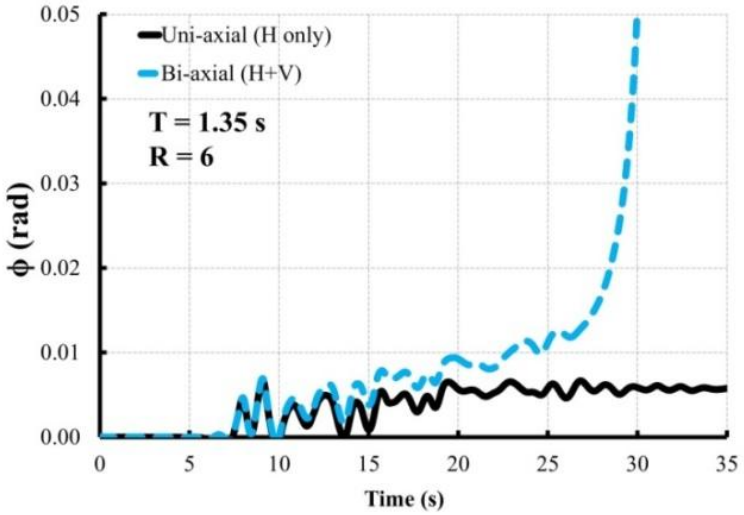

Figure 5.7: Evolution of inelastic-rotation response under uniaxial and biaxial action of Kobe earthquake recorded at Port Island.

Obviously, the VCGM not only results in increased inelastic horizontal response, but also in certain cases could cause collapse. Having said this, one may argue that the presented record is a unique example. However, the mentioned phenomenon was encountered again during evaluation of Northridge earthquake, as will be presented next.

5.5.3 Event 3: Northridge Earthquake

The January 17, 1994 Northridge earthquake was a magnitude 6.69 reverse earthquake. In line with previously presented events, four of the recorded motions during the 1994 Northridge earthquake are analyzed in present study (Table 5.1). Variation of the ratio of the maximum-inelastic horizontal response under biaxial excitation to the uniaxial one, under action of four records (Table 5.1) corresponding to Northridge earthquake are shown in Figure 5.8.

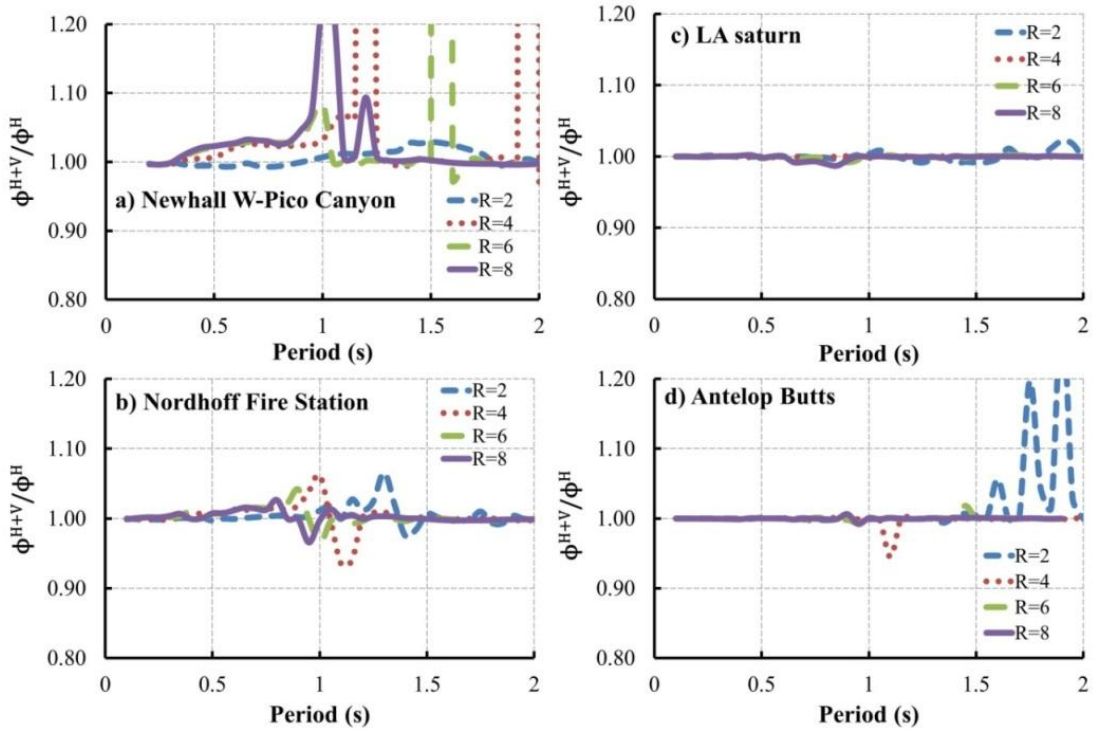

Figure 5.8: Ratio of the maximum-inelastic horizontal response under biaxial excitation to the maximum-inelastic horizontal response under uniaxial excitation under action of 1994 Northridge earthquake recorded at: a) Newhall Wpico Canyoun, b) Nordhoff Fire Station, c) LA Saturn and d) Antelop Butts.

While action of VCGM is trivial for the LA Saturn record, the Antelope Butts record shows how important the effect of VCGM might be at far-field sites. For systems with R=2, the maximum response under biaxial action of Antelope Butts record is about 20% larger than its response under uniaxial excitation. Moreover, Figures 5.8-a, b and c indicate on complications regarding influence of the strength reduction factor and initial period on the fluctuations of response under biaxial excitation.

Interesting results were obtained under action of the Newhall-Wpico Canyon record. The full range of the Figure 5.8-a, corresponding to the mentioned record is presented in Figure 5.9. It can be seen that, for certain combinations of strength reduction factor and initial period, systems under biaxial excitation loose their stability. Another example for capabality of the VCGM to cause dynamic instability.

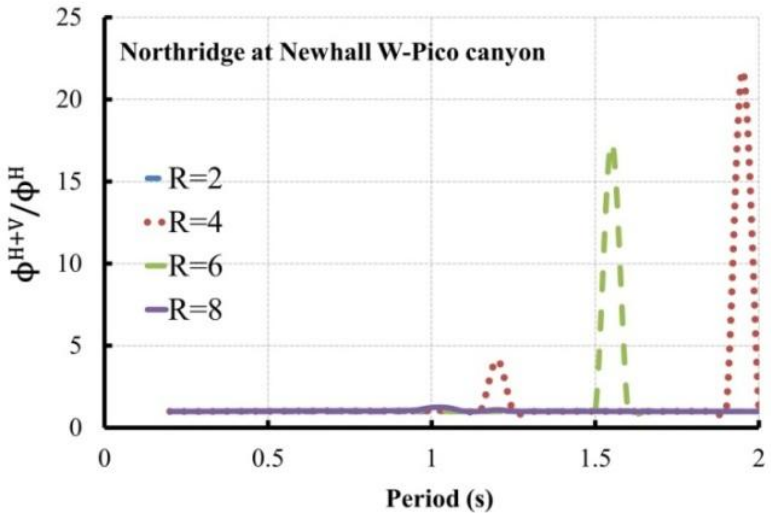

Figure 5.9: Ratio of the maximum-inelastic horizontal response under biaxial excitation to the maximum-inelastic horizontal response under uniaxial excitation under action of 1994 Northridge earthquake recorded at Newhall-Wpico Canyon.

Capability of VCGM to initiate dynamic instability is a very important issue, with significant consequences, which needs further investigation. To this end, the next step emphasizes on this phenomenon.

5.6 Capability of VCGM to Initiate Dynamic Instability

The major aim of the second step is to examine possibility of observing dynamic instability under biaxial action of a set of recorded motions, which are selected based on currently available selection and scaling strategies. To this end, the spectrum matching method implemented in the PEER-NGA2 Ground Motion Database is adopted to select and scale a set of records representing a near-field site in Turkey. All records are selected from strike slip category and geometric mean of their horizontal components is used for scaling. The adopted target spectrum and the selected bin of recorded motions were presented in Figure 5.2, and Table 5.2, respectively.

When records were selected, an important question was confronted; that is, how the vertical components should be scaled if scaled horizontal components are going to be used. Close inspection of Eq.(5.1) shows that the value of vertical acceleration directly affects the system's resistance. Hence, any method for scaling VCGM needs to be tested before implementation. Moreover, capability of current state of selecting and scaling strategies in reflecting effect of VCGM on the horizontal response is still a matter of question. To prevent undesireable bias in analysis due to misscaling the vertical components, it was decided to use the unscaled version of records. Furthermore, vertical component of one of the records was not available, hence it was eliminated from analysis; resulting in a total of 24 remaining records.

In the second step, 6 levels of R-factor (from 1 to 6) are used. In addition, and following the results of the first step, systems with initial periods between 1.0 to 2.0s are considered.

Inclusion of VCGM caused dynamic instability under action of four of the records, which are presented in Figure 5.10. This observation reconfirms potential capability of VCGM to cause collapse. Results of Figure 5.10, together with those of Kobe and Northridge earthquakes can serve as counter examples which point to importance of considering VCGM, at least for certain combinations of initial period and R-factor, in collapse evaluation.

Moreover, and as shown in Figure 5.11, significant variation of inelastic response under biaxial action of three records was observed. For the rest of records, inclusion of the VCGM resulted in insignificnt variation of horizontal response.

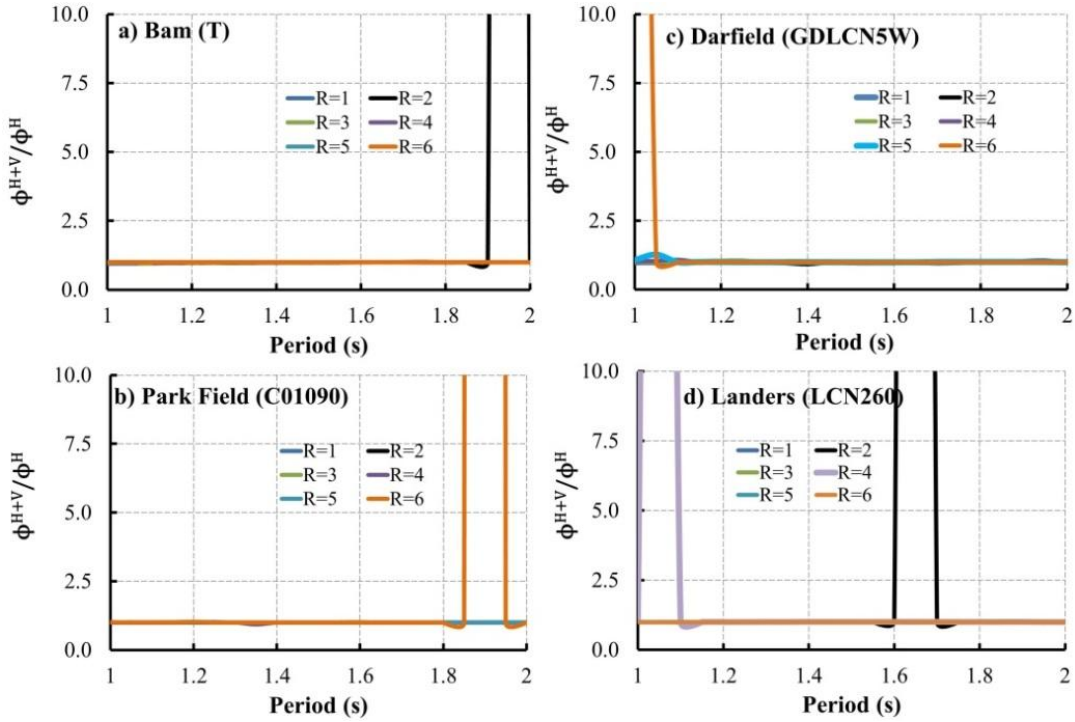

Figure 5.10: Ratio of maximum-inelastic horizontal response under biaxial excitation to the maximum-inelastic horizontal response under uniaxial excitation under action of a) Bam, b) Park Field, c) Darfield, and d) Landers.

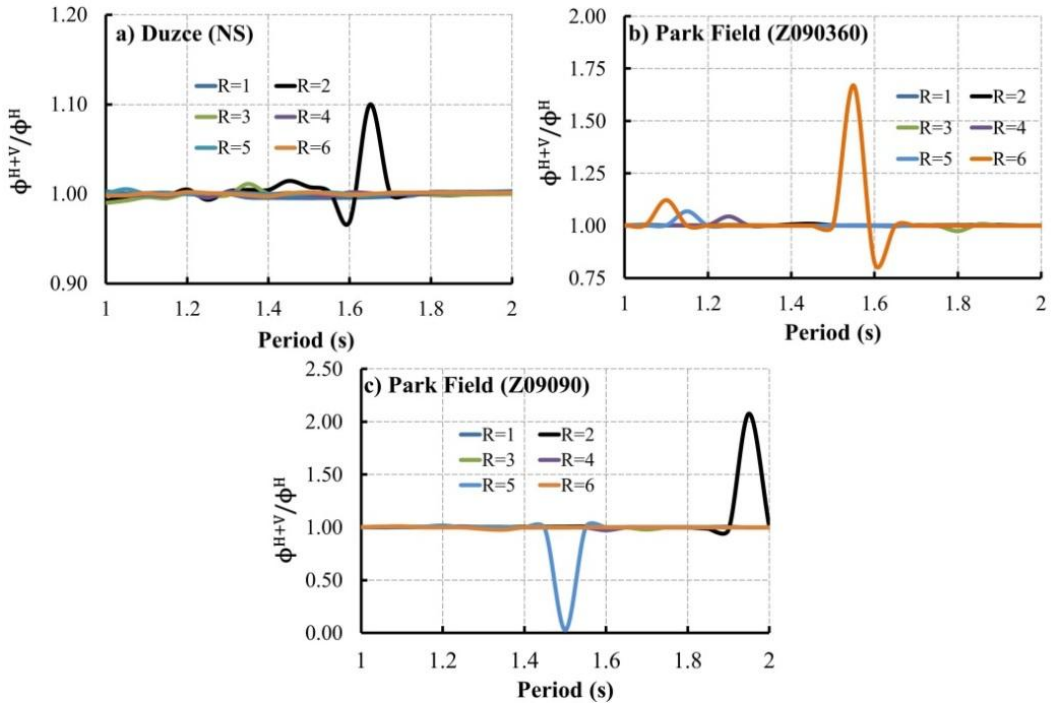

Figure 5.11: Ratio of the maximum-inelastic horizontal response under biaxial excitation to the maximum-inelastic horizontal response under uniaxial excitation under action of a) Duzce (NS) , b) Park Field Z09 (360), and c) Park Field Z09 (090).

Chapter 6

CONCLUSIONS

The present study has followed a two-fold aim. First, it has tried to present a different perspective in treating the P-delta effect by proposing an alternative response spectrum. To this end, it was noted that current code specified limits are imposed on the storey-wise SCs, not fundamental period of vibration. On the other hand, previous literature indicates that the SC is a period-dependent parameter, which presents an opportunity to plot spectral information against SC, instead of period. Such spectra were developed based on an inverted-pendulum model and were referred to as SCRS. It was debated that such a model not only satisfies all the necessary requirements of SDOFs, but also the period-dependent feature of SC can be considered. Moreover, P-delta effect is inherent in the pendulum's governing equation of motion, and hence, its effect on the response spectra is directly considered. It was also indicated that upon adaptation of the period-dependent SC, the inverted-pendulum formulation is equivalent to the UPEM, and hence, it retains all advantages of the mentioned method in terms of consistency and accuracy.

It was discussed that unlike constant SC, using period-dependent SC prevents underestimation of the P-delta effect by increasing period. The mentioned phenomenon, which seems to be more significant for highly ductile systems, was further tested on a set of records. Results indicate on a systematic underestimation of

the P-delta effect, by use of the amplification factors; and likewise, an overestimation of the SC limit below which the P-delta effect is considered negligible.

To extend application of the SCRS to derivation of the base-shear of MDOFs, it was noted that limiting the SC at various levels of a MDOF is equivalent to imposing an upper limit on the individual-storey-periods. Among various stories of a MDOF, the first-storey is an especial case with some specific features; for instance, input motion at the first-storey is known, shear at the first-storey is equal to the base-shear, and its height rarely changes during design. The mentioned properties permit introduction of a new SDOF system, namely: the FSSDOF system, with further practical advantages. It should be noted that the FSSDOF system is not aimed to simulate dynamic characteristics of the original MDOF system; rather, it is a practical tool that enables extension of the SCRS to calculation of the base-shear of MDOF systems. Further, it was discussed that derivation of a modified version of the YPS, in which the period-dependent feature of SC is considered, permits accounting for the drift-ratio limits at early stages of a design project.

On the other hand, the maximum calculated SC, or drift ratio, does not necessarily occur at the first-storey. However, the use of the SCRS and FSSDOF system permits setting the minimum necessary lateral stiffness, complying with the code specified limits, at the very early stages of design.

It is worth mentioning that since present study focuses on design of new structures, in developing the presented discussions only bilinear material behavior with 5% hardening and 5% damping were used. Moreover, for assessing the suitability of the amplification factors a set of strike-slip earthquakes recorded at near field was used.

In addition, applicability of the FSSDOF system was tested on regular SMRFs. Thus, based on the presented discussions, and limited to the adopted assumptions, it can be concluded that:

- Consideration of the P-delta effect in both strength based, and displacement based design approaches can be enhanced by using an alternative response spectrum in terms of SC, instead of fundamental period of vibration.
- The notion of SCRS permits accounting for the SC limits from early stages of a design process.
- By use of the notion of FSSDOF system, it is possible to set the minimum necessary lateral stiffness, complying with a given ductility, and based on the code specified limits, from early stages of a design process.
- The modified YPS provides an opportunity to account for the drift ratio limits. Thus, it facilitates using the FSSDOF in the DDBD context.

Second, the fifth chapter has investigated possible effects of the VCGM on the maximum-inelastic horizontal response. Since available record selection methods rely on uncoupled vibratos in horizontal and vertical directions, present study has followed two steps. In the first step, an event-based record selection has been adopted, while the second step has followed an available selection strategy. Moreover, initial period of vibration, strength reduction factor, and distance to source has been used as engineering variables for this investigation.

Based on presented discussions, and limited to the range of investigated parameters, below conclusions can be drawn:

- For some combinations of the initial period of vibration and strength reduction factor, inclusion of the VCGM significantly affects the maximum-inelastic-horizontal-response of SDOF systems. This is due to variation of the P-delta effect because of variation of gravitational acceleration. The mentioned effect is significant for systems with initial periods ranging approximately from 1.0 to 2.0 s. This was attributed to period-dependent feature of SC.
- Effect of the VCGM on the maximum-inelastic-horizontal-response is not limited to near field regions.
- The presented examples suggest that inclusion of VCGM may cause an increase or decrease in the imposed ductility demand; hence, attributing all the observed damage resulting from increased ductility demand to the horizontal component of ground motion may cause misevaluation.
- Although previous literature qualitatively discusses the potential capabilities of the VCGM to initiate dynamic instability, present investigation presents specific examples of occurrence of dynamic instability. Therefore, it suggests consideration of the VCGM for collapse evaluation.

Furthermore, in the third chapter the geometrically linear and nonlinear equations of motion were compared. Based on whether SC is equal to or greater than material hardening two major cases were considered. Based on the presented results, and limited to the range of adopted parameters, it can be concluded that:

- When the SC is equal to the material hardening including the geometric nonlinearity will significantly affect the calculated ductility demand. This issue becomes especially important for estimating the maximum-inelastic-

rotations (displacements). It was also found that variation of the relative strength and frequency and amplitude of the excitation affect the differences in calculated ductility demands.

- On the other hand, in addition to the calculated ductility demands, when the SC is larger than material hardening the differences between the two formulations are manifested in terms of the stability of the solution. While the geometrically linear system loses its stability, the geometrically nonlinear system shows stable behavior. This phenomenon might enhance the convergence problems encountered in applications dealing with large displacements. Furthermore, it will enhance a more detailed understanding of full range behavior of a system, from elastic to inelastic, and, eventually to collapse stage.

Further investigation of the possible effects of the VCGM on real structures might be performed in light of the results of present study. Moreover, the SCRS and FSSDOF might be further extended to irregular MDOFs.

REFERENCES

Adam, C., & Ibarra, L. (2015). Seismic collapse assessment. *Encyclopedia of Earthquake Engineering 3*, 2729-2752.

Adam, C., Ibarra, L. F., & Krawinkler, H. (2004). *Evaluation of P-delta effects in non-deteriorating MDOF structures from equivalent SDOF systems*. Paper presented at the 13th World Conference on Earthquake Engineering, Vancouver, B. C., Canada.

Adam, C., & Jäger, C. (2012a). Seismic collapse capacity of basic inelastic structures vulnerable to the P-delta effect. *Earthquake Engineering & Structural Dynamics, 41*(4), 775-793.

Adam, C., & Jäger, C. (2012b). Simplified collapse capacity assessment of earthquake excited regular frame structures vulnerable to P-delta. *Engineering Structures, 44*, 159-173.

Amara, F., Bosco, M., Marino, E. M., & Rossi, P. P. (2014). An accurate strength amplification factor for the design of SDOF systems with P–Δ effects. *Earthquake Engineering & Structural Dynamics, 43*(4), 589-611.

Andrews, A. (1977). Slenderness Effects in Earthquake Resisting Frames *Bulletin of New Zealand National Society for Earthquake Engineering 10*(3), 71-75.

ASCE/SEI. (2010). *minimum design loads for buidings and other structures*. Reston VA: American Society of Civil Engineers/Structural Engineering Institute.

Aschheim, M., & Black, E. F. (2000). Yield point spectra for seismic design and rehabilitation. *Earthquake Spectra, 16*(2), 317-336.

Aschheim, M., & Montes, E. H. (2003). The representation of P-Δ effects using Yield Point Spectra. *Engineering structures, 25*(11), 1387-1396.

Asimakopoulos, A. V., Karabalis, D. L., & Beskos, D. E. (2007). Inclusion of P–Δ effect in displacement-based seismic design of steel moment resisting frames. *Earthquake Engineering & Structural Dynamics, 36*(14), 2171-2188.

Aydınoğlu, M., & Fahjan, Y. (2003). A unified formulation of the piecewise exact method for inelastic seismic demand analysis including the P-delta effect. *Earthquake Engineering & Structural Dynamics, 32*(6), 871-890.

Baker, J. W., & Lee, C. (2017). An Improved Algorithm for Selecting Ground Motions to Match a Conditional Spectrum. *Journal of Earthquake Engineering*, 1-16.

Belleri, A., Torquati, M., Marini, A., & Riva, P. (2017). A Novel Framework to Include P-Δ Effects in Displacement-Based Seismic Assessment. *Journal of Earthquake Engineering, 21*(3), 486-492.

Bernal, D. (1987). Amplification factors for inelastic dynamic p–Δ effects in earthquake analysis. *Earthquake Engineering & Structural Dynamics, 15*(5), 635-651.

Bernal, D. (1992). Instability of buildings subjected to earthquakes. *Journal of Structural Engineering, 118*(8), 2239-2260.

Bernal, D. (1998). Instability of buildings during seismic response. *Engineering Structures, 20*(4), 496-502.

Black, E. (2011). Use of stability coefficients for evaluating the P–Δ effect in regular steel moment resisting frames. *Engineering Structures, 33*(4), 1205-1216.

Bommer, J., Spence, R., Erdik, M., Tabuchi, S., Aydinoglu, M., Booth, E., . . . Peterken, O. (2002). Development of an earthquake loss model for Turkish catastrophe insurance. *Journal of Seismology*, *6*(3), 431-446.

Bozorgnia, Y., & Campbell, K. W. (2004). The vertical-to-horizontal response spectral ratio and tentative procedures for developing simplified V/H and vertical design spectra. *Journal of Earthquake Engineering, 8*(02), 175-207.

Bozorgnia, Y., & Campbell, K. W. (2016). Vertical ground motion model for PGA, PGV, and linear response spectra using the NGA-West2 database. *Earthquake Spectra, 32*(2), 979-1004.

Çağnan, Z., Akkar, S., Kale, Ö., & Sandıkkaya, A. (2017). A model for predicting vertical component peak ground acceleration (PGA), peak ground velocity (PGV), and 5% damped pseudospectral acceleration (PSA) for Europe and the Middle East. *Bulletin of Earthquake Engineering, 15*(7), 2617-2643.

Campbell, K. W. (2003). Prediction of strong ground motion using the hybrid empirical method and its use in the development of ground-motion (attenuation) relations in eastern North America. *Bulletin of the Seismological Society of America, 93*(3), 1012-1033.

Campbell, K. W., & Bozorgnia, Y. (2003). Updated near-source ground-motion (attenuation) relations for the horizontal and vertical components of peak ground acceleration and acceleration response spectra. *Bulletin of the Seismological Society of America, 93*(1), 314-331.

CEN. (2005). *Design of structures for earthquake resistance-Part 1: General rules, seismic actions and rules for buildings*.

Chopra, A. K. (2007). *Dynamics of structures: theory and applications to earthquake engineering. 2007*: Prentice-Hall.

Collier, C., & Elnashai, A. (2001). A procedure for combining vertical and horizontal seismic action effects. *Journal of Earthquake Engineering, 5*(04), 521-539.

Dobson, S., Noori, M., Hou, Z., Dimentberg, M., & Baber, T. (1997). Modeling and random vibration analysis of SDOF systems with asymmetric hysteresis. *International Journal of Non-Linear Mechanics, 32*(4), 669-680.

Elgamal, A., & He, L. (2004). Vertical earthquake ground motion records: an overview. *Journal of Earthquake Engineering, 8*(05), 663-697.

Elnashai, A., & Papazoglou, A. (1997). Procedure and spectra for analysis of RC structures subjected to strong vertical earthquake loads. *Journal of Earthquake Engineering, 1*(01), 121-155.

Erdik, M. (2001). Report on 1999 Kocaeli and Düzce (Turkey) earthquakes *Structural Control for Civil and Infrastructure Engineering* (pp. 149-186): World Scientific.

Erdik, M., & Nuray Aydinoglu, M. (2011). Rehabilitation, Recovery and Preparedness after 1999 Kocaeli and Duzce Earthquakes *Natural Disaster Reduction in the 21st Century* (pp. 7-12): Thomas Telford Publishing.

FEMA. (2009). *NEHRP recommended seismic provisions for new buildings and other structures (FEMA P-750)*. Washington, DC: Federal Emergency Management Agency.

Foschaar, J., Baker, J., & Deierlein, G. (2012). *Preliminary assessment of ground motion duration effects on structural collapse.* Paper presented at the Proceedings of the 15th world conference on earthquake engineering.

Ghaffarzadeh, H., & Nazeri, A. (2015). The effect of the vertical excitation on horizontal response of structures. *Earthquakes and Structures, 9*(3), 625-637.

Graizer, V., & Kalkan, E. (2008). Response of pendulums to complex input ground motion. *Soil Dynamics and Earthquake Engineering, 28*(8), 621-631.

Gupta, A., & Krawinkler, H. (2000). Dynamic P-delta effects for flexible inelastic steel structures. *Journal of Structural Engineering, 126*(1), 145-154.

Haselton, C., Whittaker, A., Hortacsu, A., Baker, J., Bray, J., & Grant, D. (2012). *Selecting and scaling earthquake ground motions for performing response-history analyses*. Paper presented at the Proceedings of the 15th World Conference on Earthquake Engineering.

Haselton, C. B., & Deierlein, G. G. (2008). *Assessing seismic collapse safety of modern reinforced concrete moment-frame buildings*: Pacific Earthquake Engineering Research Center.

Haselton, C. B., Liel, A. B., & Deierlein, G. G. (2009). *Simulating structural collapse due to earthquakes: model idealization, model calibration, and numerical solution algorithms.* Paper presented at the Computational Methods in Structural Dynamics and Earthquake Engineering (COMPDYN).

Hjelmstad, K., & Williamson, E. (1998). Dynamic stability of structural systems subjected to base excitation. *Engineering Structures, 20*(4), 425-432.

Horwich, G. (2000). Economic lessons of the Kobe earthquake. *Economic Development and Cultural Change, 48*(3), 521-542.

Ibarra, L., & Krawinkler, H. (2011). Variance of collapse capacity of SDOF systems under earthquake excitations. *Earthquake Engineering & Structural Dynamics, 40*(12), 1299-1314.

Ibarra, L. F., & Krawinkler, H. (2004). *Global collapse of deteriorating MDOF systems.* Paper presented at the 13th World Conference on Earthquake Engineering, Vancouver, BC, Canada.

Ibarra, L. F., Medina, R. A., & Krawinkler, H. (2005). Hysteretic models that incorporate strength and stiffness deterioration. *Earthquake engineering & structural dynamics, 34*(12), 1489-1511.

Ismail, M., Ikhouane, F., & Rodellar, J. (2009). The hysteresis Bouc-Wen model, a survey. *Archives of Computational Methods in Engineering, 16*(2), 161-188.

Jäger, C., & Adam, C. (2013). Influence of collapse definition and near-field effects on collapse capacity spectra. *Journal of Earthquake Engineering, 17*(6), 859-878.

Jennings, P. C., & Husid, R. (1968). Collapse of yielding structures during earthquakes. *Journal of Engineering Mechanics*.

Jough, F. K. G., & Şensoy, S. (2016). Prediction of seismic collapse risk of steel moment frame mid-rise structures by meta-heuristic algorithms. *Earthquake Engineering and Engineering Vibration, 15*(4), 743-757.

Kalkan, E., & Graizer, V. (2007). Coupled tilt and translational ground motion response spectra. *Journal of Structural Engineering, 133*(5), 609-619.

Kim, S. J., Holub, C. J., & Elnashai, A. S. (2010). Analytical assessment of the effect of vertical earthquake motion on RC bridge piers. *Journal of Structural Engineering, 137*(2), 252-260.

Kunnath, S. K., Erduran, E., Chai, Y., & Yashinsky, M. (2008). Effect of near-fault vertical ground motions on seismic response of highway overcrossings. *Journal of Bridge Engineering, 13*(3), 282-290.

Liel, A. B., Haselton, C. B., Deierlein, G. G., & Baker, J. W. (2009). Incorporating modeling uncertainties in the assessment of seismic collapse risk of buildings. *Structural Safety, 31*(2), 197-211.

López, S. E., Ayala, A. G., & Adam, C. (2015). A novel displacement-based seismic design method for framed structures considering P-Delta induced dynamic instability. *Bulletin of Earthquake Engineering, 13*(4), 1227-1247.

MacRae, G. A. (1994). P-Δ effects on single-degree-of-freedom structures in earthquakes. *Earthquake Spectra, 10*(3), 539-568.

Miranda, E. (2000). Inelastic displacement ratios for structures on firm sites. *Journal of Structural Engineering, 126*(10), 1150-1159.

Miranda, E., & Akkar, S. D. (2003). Dynamic instability of simple structural systems. *Journal of Structural Engineering, 129*(12), 1722-1726.

Miranda, E., & Ruiz-García, J. (2002). Evaluation of approximate methods to estimate maximum inelastic displacement demands. *Earthquake engineering & structural dynamics, 31*(3), 539-560.

Newmark, N. M., Blume, J. A., & Kapur, K. K. (1973). Seismic design spectra for nuclear power plants. *Consulting Engineering Services, Urbana, IL*.

Papadrakakis, M., Fragiadakis, M., Lagaros, N. D., & Plevris, V. (2011). *Computational methods in earthquake engineering*: Springer.

Papazoglou, A., & Elnashai, A. (1996). Analytical and field evidence of the damaging effect of vertical earthquake ground motion. *Earthquake Engineering and Structural Dynamics, 25*(10), 1109-1138.

Paulay, T. (1978). A consideration of P-delta effects in ductile reinforced concrete frames. *Bulletin of the New Zealand National Society for Earthquake Engineering, 11*(3), 151-160.

Priestley, M. (2000). Performance based seismic design. *Bulletin of the New Zealand society for earthquake engineering, 33*(3), 325-346.

Priestley, M., Calvi, G., & Kowalsky, M. (2007). *Direct displacement-based seismic design of structures*. Paper presented at the Proceedings of the 2007 NZSEE conference.

Rabiei, M., & Khoshnoudian, F. (2011). Response of multistory friction pendulum base-isolated buildings including the vertical component of earthquakes. *Canadian Journal of Civil Engineering, 38*(10), 1045-1059.

Rahimi, E., & Estekanchi, H. (2015). Collapse assessment of steel moment frames using endurance time method. *Earthquake Engineering and Engineering Vibration, 14*(2), 347-360.

Rosenblueth, E. (1965). Slenderness effects in buildings. *Journal of the Structural Division, 91*(1), 229-252.

Ruiz-García, J., & Miranda, E. (2003). Inelastic displacement ratios for evaluation of existing structures. *Earthquake Engineering & Structural Dynamics, 32*(8), 1237-1258.

Shi, W., Lu, X., Guan, H., & Ye, L. (2014). Development of seismic collapse capacity spectra and parametric study. *Advances in Structural Engineering, 17*(9), 1241-1255.

Sivaselvan, M. V., & Reinhorn, A. M. (2000). Hysteretic models for deteriorating inelastic structures. *Journal of Engineering Mechanics, 126*(6), 633-640.

Sun, C.-K., Berg, G. V., & Hanson, R. D. (1973). Gravity effect on single-degree inelastic system. *Journal of the Engineering Mechanics Division, 99*(1), 183-200.

TEC. (2018). Specification for structures to be built in disaster areas. Turkey: Ministry of Public Works and Settlement

Tjondro, J., Moss, P., & Carr, A. (1992). Seismic P-δ effects in mesium height moment resisting steel frames. *Engineering structures, 14*(2), 75-90.

Vamvatsikos, D., & Cornell, C. A. (2002). Incremental dynamic analysis. *Earthquake Engineering & Structural Dynamics, 31*(3), 491-514.

Wei, B., Xu, Y., & Li, J. (2011). Treatment of P-Δ effects in displacement-based seismic design for SDOF systems. *Journal of Bridge Engineering, 17*(3), 509-518.

Williamson, E. B. (2003). Evaluation of damage and P-Δ effects for systems under earthquake excitation. *Journal of Structural Engineering, 129*(8), 1036-1046.

Williamson, E. B., & Hjelmstad, K. D. (2001). Nonlinear dynamics of a harmonically-excited inelastic inverted pendulum. *Journal of Engineering Mechanics, 127*(1), 52-57.

Zareian, F., Krawinkler, H., Ibarra, L., & Lignos, D. (2010). Basic concepts and performance measures in prediction of collapse of buildings under earthquake

ground motions. *The Structural Design of Tall and Special Buildings, 19*(1-2), 167-181.